AD-A098 885 NAVAL RESEARCH LAB WASHINGTON DC F/G 20/5
LINEAR AND NONLINEAR ELECTRON CYCLOTRON INTERACTION IN OPEN RES--ETC(U)
MAY 81 J L VOMVORIDIS, P SPRANGLE
UNCLASSIFIED NRL-MR-4459 NL

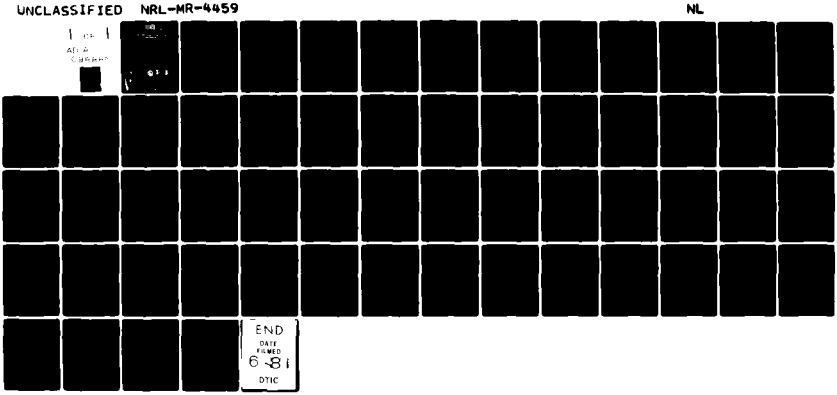

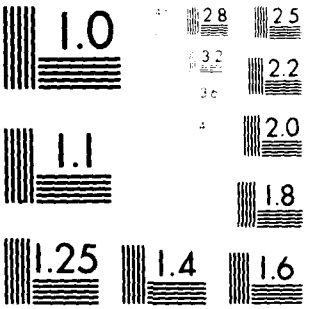

MICROCOPY RESOLUTION TEST CHART

NRL Memorandum Report 4459

AD A098885

Linear and Nonlinear Electron Cyclotron Interaction in Open Resonators

J. L. VOMVORIDIS

JAYCOR
Alexandria, VA 22304

and

P. SPRANGLE

Plasma Theory Branch
Plasma Physics Division

May 7, 1981

NAVAL RESEARCH LABORATORY
Washington, D.C.

Approved for public release; distribution unlimited.

9 Memorandum report

SECURITY CLASSIFICATION OF THIS PAGE (When Data Entered)

REPORT DOCUMENTATION PAGE	READ INSTRUCTIONS BEFORE COMPLETING FORM
1. REPORT NUMBER: NRL Memorandum Report 4459 (14) NRL-MR-4	2. GOVT ACCESSION NO.: AD-A098 885	3. RECIPIENT'S CATALOG NUMBER
4. TITLE (and Subtitle): (6) LINEAR AND NONLINEAR ELECTRON CYCLOTRON INTERACTION IN OPEN RESONATORS.	5. TYPE OF REPORT & PERIOD COVERED: Interim report on a continuing NRL problem.
	6. PERFORMING ORG. REPORT NUMBER
7. AUTHOR(s): (10) J. L. Vomvoridis* and P. Sprangle (11) 7 May 81	8. CONTRACT OR GRANT NUMBER(s)
9. PERFORMING ORGANIZATION NAME AND ADDRESS: Naval Research Laboratory Washington, DC 20375 (12) 58	10. PROGRAM ELEMENT, PROJECT, TASK AREA & WORK UNIT NUMBERS: 47-0865-0-1
11. CONTROLLING OFFICE NAME AND ADDRESS: Department of Energy Washington, DC 20545	12. REPORT DATE: May 7, 1981
	13. NUMBER OF PAGES: 56
14. MONITORING AGENCY NAME & ADDRESS (if different from Controlling Office)	15. SECURITY CLASS. (of this report): UNCLASSIFIED
	15a. DECLASSIFICATION/DOWNGRADING SCHEDULE

16. DISTRIBUTION STATEMENT (of this Report)

Approved for public release; distribution unlimited.

17. DISTRIBUTION STATEMENT (of the abstract entered in Block 20, if different from Report)

18. SUPPLEMENTARY NOTES

*Present address: JAYCOR, Alexandria, VA 22304

19. KEY WORDS (Continue on reverse side if necessary and identify by block number)

Relativistic electron-cyclotron-maser
Electron cyclotron beam
Plane wave radiation
Beam-wave interaction
Open resonator

20. ABSTRACT (Continue on reverse side if necessary and identify by block number)

In this work the electron cyclotron maser oscillator interaction is analyzed in an open resonator configuration. One of the salient features of this configuration for generating high power short wavelength radiation is its ability to mode select. Both the linear and nonlinear analysis are developed for an arbitrary value of the refractive index $n = kc/\omega$. Specializing to luminous waves, $n \to 1$, it is shown that the linear gain curve is symmetric

as [illegible] to 1

(Continues)

DD FORM 1 JAN 73 1473 EDITION OF 1 NOV 65 IS OBSOLETE
S/N 0102-014-6601

SECURITY CLASSIFICATION OF THIS PAGE (When Data Entered)

251 159

20. ABSTRACT (Continued)

about synchronism and that instability can occur even at exact synchronism, for appropriate initial beam distributions. The nonlinear integrals of the motion are obtained, indicating that the total energy is available, the nonlinear evolution is described by a single differential equation, and the nonlinear efficiency is shown to depend on only four combinations of the beam, field, and resonator parameters. Nonlinear efficiencies up to 15% can be achieved. For a relativistic beam, a substantial frequency upshift is possible, with efficiencies up to 10%. Efficiency enhancement is possible, e.g., by the introduction of a two-stage resonator. In such a configuration, efficiencies exceeding 30% are calculated. Finally, the requirements for beam temperature and mode selectivity are found not to be particularly restrictive.

CONTENTS

I. INTRODUCTION 1

II. LINEAR THEORY 6

III. NONLINEAR THEORY 17

IV. *DISCUSSION* 35

ACKNOWLEDGMENTS 44

REFERENCES 45

Accession For
NTIS GRA&I ☑
DTIC TAB ☐
Unannounced ☐
Justification
By
Distribution/
Availability Codes
Dist | Avail and/or Special
A

LIST OF FIGURES

1. Schematic representation of the quasi-optical resonator 2
2. Linear efficiency vs. resonator length 15
3. Phase space trajectories 23
4. Comparison of phase space trajectories 25
5. Contour plots for the efficiency coefficient C_η 28
6. Contour plots for the anisotropy constant C_d 29
7. Spatial evolution of the normalized efficiency 31
8. Contour plots of the normalized efficiency 32
9. Optimal normalized efficiency 34
10. Efficiency enhancement in a two-stage oscillator configuration 42

LINEAR AND NONLINEAR ELECTRON CYCLOTRON INTERACTION IN OPEN RESONATORS

I. INTRODUCTION

One of the most recently developed devices for the generation of coherent radiation in the millimeter and centimeter range is the gyrotron (or, electron cyclotron maser). In this device, radiation power is produced by the interaction of the TE fields of the cavity with an electron beam which propagates and gyrates along an external static magnetic field. This interaction has been studied extensively,[1-18] both theoretically and experimentally, with impressive results, such as a 22% efficiency of conversion of beam kinetic power to radiation at a 2 mm wavelength with 22 kW CW output power. Substantial improvements are possible if axial nonuniformities are introduced in the form of gradients either in the oscillator cross-section,[19,20] or in the external magnetic field.[21-23]

The frequency of the gyrotron is determined by the relativistic gyrofrequency of the electrons in the external magnetic field. For efficient operation, this gyrofrequency, Doppler-shifted in the electron beam rest frame, must be in close synchronism with the eigenfrequency of the cavity. However, since the size of the cavity cannot be made arbitrarily small, a large value of the gyrofrequency may result in synchronism with more than one of the cavity eigenfrequencies. Although preliminary investigations[24-28] have not been conclusive, it is expected that multi-mode effects may prove a problem for wavelengths less than $\sim$1 mm.

To avoid such potential limitations, it is proposed that the gyrotron cavity be replaced by an open quasi-optical resonator, Fig. 1, formed by two mirrors of approriate shape. Taking the z-axis as the axis of the radiation, the fields can be shown to be derivable from the usual vector potential

Manuscript submitted March 10, 1981.

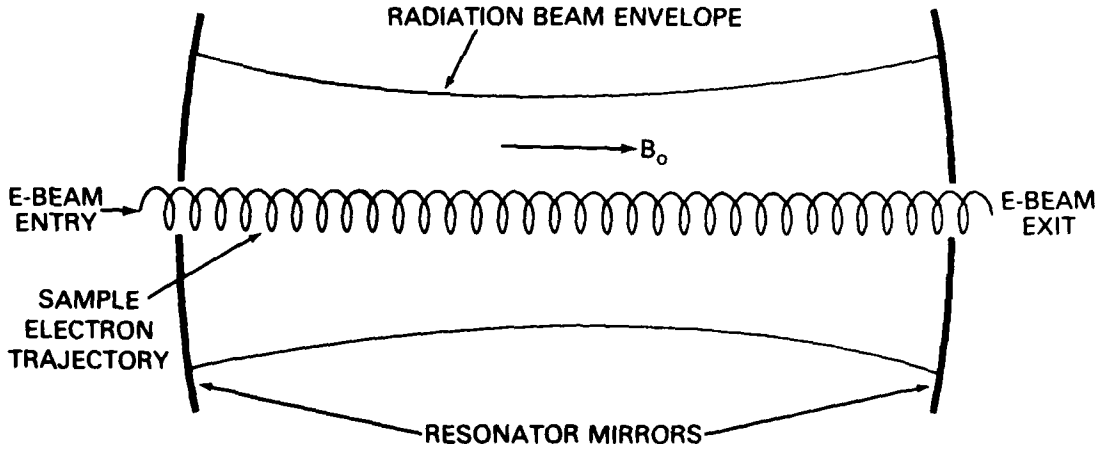

Fig. 1 — Schematic representation of the quasi-optical resonator and electron beam configuration. The diffracted fields are contained by the two mirrors, one or both of which may be partially transmitting. The individual electrons of the beam execute, to zero order, a helical motion in the external magnetic field B_o.

$$\underline{A} = 2A(r,z)\sin\left[kz + \alpha(r,z)\right]\left[\hat{\underline{e}}_x \cos(\omega t) + \varepsilon\hat{\underline{e}}_y \sin(\omega t)\right]$$
$$+ \frac{2}{kr}\frac{\partial}{\partial r}\left[A\cos(kz + \alpha)\right]\left[x\cos(\omega t) + \varepsilon y \sin(\omega t)\right]\hat{\underline{e}}_z \tag{1}$$

where ω is the radiation frequency, $k = \omega/c$ is the dominant term of the wavenumber, $\alpha(r,z) = kr^2/2R + \tan^{-1}(z/z_0)$ is the spatially dependent phase, $A(r,z) = A_0(r_0/r_s)\exp(-r^2/r_s^2)$ is the position dependent amplitude for the fundamental mode, ε is the ellipticity of the radiation, $r = (x^2 + y^2)^{\frac{1}{2}}$ is the transverse coordinate, $r_s(z) = r_0(1 + z^2/z_0^2)$ is the spot size at z with r_0 its minimum value at z=0, $R(z) = z(1 + z_0^2/z^2)$ is the radius of curvature of the wave front at z, $z_0 = \pi r_0^2/\lambda$ is the Rayleigh length, and $\lambda = 2\pi/k$ is the wavelength. The diffraction angle of the fundamental mode is $\Theta_d = \lambda/\pi r_0$. The diffraction angle of the higher order modes is larger. Therefore, if the radius of the mirrors is somewhat larger than r_s, most of the energy of the fundamental mode will be intercepted, resulting in a high value of Q. The higher order modes on the other hand will suffer from diffraction losses, their Q's will be small, and therefore these modes will not be excited. Thus the introduction of open resonators provides an effective natural means for transverse mode selection.

This paper is intended as a preliminary but comprehensive analysis of the electron cyclotron interaction with the diffracted fields of Eq. (1). The limit we have considered throughout the paper is that of an electron beam propagating along the radiation axis.[29] We have assumed that the transverse extent of the beam is small compared to the radiation spot size r_s, therefore the action of the field on the beam electrons is that of a plane wave. In this limit we have developed the linear theory

(Sec. II) and the nonlinear theory (Sec. III) of the interaction in a bounded system (oscillator). Various issues pertaining to the basic theory are discussed in Sec. IV, along with the presentation of numerical examples.

In Section II the linear dispersion relation is obtained for an oscillator. For the sake of generality, an arbitrary electron beam distribution is assumed. All forward and backward components of the field perturbation are kept and the value of the refractive index $n = kc/\omega$ is left unspecified in the bulk of the analysis in this Section. Specializing to the case of a monoenergetic beam, affected only by the forward wave,[30] yields a compact result and reproduces the expressions for the gyrotron in the cut-off frame, when $n \to 0$. For luminous waves, $n \to 1$, the gain curve has two interesting features, viz. it possesses even symmetry about the frequency of synchronism and can lead to instability even at exact synchronism, provided that the transverse beam velocity satisfies a certain inequality.

The nonlinear theory is developed in Section III for a constant amplitude wave. The equations of motion for the electrons are expressed using the axial coordinate z as the independent Lagrangian variable. These equations are interrelated by four invariants. Two of these invariants relate the transverse displacement to the velocity, while the other two relate the velocity components. These invariants reproduce earlier results when $n \to 0$ or $n > 1$. A transformation to slowly varying variables eliminates an additional variable and results in a single integrable equation. The phase space plots are studied and distinction between closed and open orbits is made. A condition for complete electron

kinetic energy depletion is identified. The nonlinear efficiency is found to depend on only four combinations of the field and electron beam parameters and is conveniently presented in contour plots.

Finally, certain aspects related to the applicability of our analysis are discussed in Section IV. It is shown that the symmetry of the gain spectrum can be used to relax the temperature requirements. The interaction is also shown to have inherent abilities for axial mode selection. In our example of a gyrotron type operation we obtained a 13.7% efficiency at $\lambda = 2$ mm with a 61 kW output power. The potential application of this interaction as a free-electron laser is discussed and a scheme for efficiency enhancement is proposed. By utilizing a two-oscillator configuration, an efficiency $\eta = 35\%$ is obtained, while estimates predict efficiencies can reach 60%.

The cyclotron interaction of electrons with luminous waves has been the subject of two recent investigations.[31,32] In the first paper the dispersion relation was obtained and analyzed for waves with arbitrary values of $n = kc/\omega$ in the limit of vanishing axial beam velocity. In the second paper the stability was investigated in terms of particle energy loss, obtained from an expansion of the equations of motion in the radiation field amplitude. Both these analyses assume a uniform medium of infinite extend in z and use the time as the independent coordinate. Accordingly, their results differ from ours, since in the present work the axial position z is used as the independent variable and the presence of the oscillator boundaries is important.

II. LINEAR THEORY

The fields of the oscillator are given in terms of the vector potential $\underset{\sim}{A}$ by the simplification of Eq. (1),

$$\begin{aligned} \underset{\sim}{A} &= A_0 \sin(kz)\,(\hat{\underset{\sim}{e}}_x + i\varepsilon\,\hat{\underset{\sim}{e}}_y)\,e^{-i\omega t} + \text{c.c.} \\ &= 2A_0 \sin(kz)\left[\hat{\underset{\sim}{e}}_x \cos(\omega_R t) + \varepsilon\,\hat{\underset{\sim}{e}}_y \sin(\omega_R t)\right]e^{\Gamma t}, \end{aligned} \tag{2}$$

where A_0 is the amplitude, k is the axial wavenumber (along the z axis), ω is the complex frequency consisting of the real frequency and the growth rate, $\omega = \omega_R + i\Gamma$, ε characterizes the ellipticity of the polarization, and $\hat{\underset{\sim}{e}}_x$ and $\hat{\underset{\sim}{e}}_y$ are unit transverse vectors. The oscillator fields $\delta\underset{\sim}{E}$ and $\delta\underset{\sim}{B}$ are given by

$$\begin{aligned} \delta\underset{\sim}{E} &= -\frac{1}{c}\frac{\partial \underset{\sim}{A}}{\partial t} = i\,\frac{\omega}{c}\,A_0 \sin(kz)\,(\hat{\underset{\sim}{e}}_x + i\varepsilon\,\hat{\underset{\sim}{e}}_y)\,e^{-i\omega t} + \text{c.c.}, \\ \delta\underset{\sim}{B} &= \underset{\sim}{\nabla} \times \underset{\sim}{A} = -\,ikA_0 \cos(kz)\,(\varepsilon\hat{\underset{\sim}{e}}_x + i\hat{\underset{\sim}{e}}_y)\,e^{-i\omega t} + \text{c.c.} \end{aligned} \tag{3}$$

In addition, a static uniform axial magnetic field is present, $\underset{\sim}{B}_0 = B_0\hat{\underset{\sim}{e}}_z$.

The fields given by Eq. (3) are appropriate for those in an oscillator formed by two parallel plates of infinite extent in the transverse direction. They are also applicable to a general case of an oscillator consisting of two concave boundaries, provided that A_0 and k are appropriate functions of x, y, and z and the small axial field components are included. These modifications depend on the waist of the radiation field, r_0, and the Rayleigh length $z_0 = \omega r_0^2/2c$ and are negligible if the beam width and

the electron Larmor radius are small compared to r_o, and if the axial interaction length is small compared to z_o. Accordingly, under such conditions the fields in Eq. (3) can be used with A_o and k constant.

The behavior of the field is governed by the wave equation,

$$- \nabla^2 \underset{\sim}{A} + \frac{1}{c^2} \left(\frac{\partial^2}{\partial t^2} + \nu \frac{\partial}{\partial t}\right) \underset{\sim}{A} = \frac{4\pi}{c} \underset{\sim}{J} , \tag{4}$$

where ν is a real quantity representing losses. It will be shown later that $\nu = \omega_R/Q$, where Q is the quality factor of the resonator. Expressing the current density as

$$\underset{\sim}{J} = \underset{\sim}{\tilde{J}}\, e^{-i\omega t} + \text{c.c.}, \tag{5}$$

it is found that Eq. (4) together with Eq. (2) can be put in the form

$$\frac{L}{2} \left[(k^2c^2 - \omega_R^2) - i(2\Gamma + \nu)\omega_R\right] A_o(\underset{\sim}{\hat{e}}_x + i\varepsilon\underset{\sim}{\hat{e}}_y) = \int_0^L 4\pi c\, \underset{\sim}{\tilde{J}} \sin(kz)dz, \tag{6}$$

where L is the interaction length.

Before continuing, it is necessary to evaluate ν in Eq. (6). This is accomplished by integrating Poynting's theorem along the interaction region,

$$\frac{\partial}{\partial t} \int_0^L u dz + S_z(z=L) - S_z(z=0) = - \int_0^L \delta\underset{\sim}{E}\cdot\underset{\sim}{J}\, dz, \tag{7}$$

where u is the radiation energy density and the z component of Poynting's vector S_z vanishes at z=0 and has the value $S_z = (\omega_R/Q) \int_0^L u dz$ at z=L, by the definition of Q. The definition of Γ implies an exponential variation, $\exp(2\Gamma t)$, for the energy, thus

$$(2\Gamma + \frac{\omega_R}{Q}) \int_0^L u dz = - \int_0^L \delta \underset{\sim}{E} \cdot \underset{\sim}{J} \, dz \ , \tag{8}$$

and from a comparison with Eq. (6) it is seen that

$$\nu = \frac{\omega_R}{Q} \ . \tag{9}$$

The current density in Eq. (6) will be evaluated from the appropriate moment of the distribution function, the latter obtained from the solution of the Vlasov equation. Employing the expansion $f = f^{(0)} + f^{(1)}$ of the distribution function, $f^{(0)}$ describes the zero-order trajectories in the external magnetic field and is therefore a function of the corresponding constants of motion,

$$\begin{aligned}
p_\perp^2 &= p_x^2 + p_y^2 \ , \\
\theta &= \tan^{-1} \left(\frac{p_y}{p_x}\right) - \frac{\Omega_o m_o}{p_z} z \ , \\
p_{\parallel} &= p_z \ , \\
x_g &= x - \frac{p_y}{\Omega_o m_o} \ , \\
y_g &= y + \frac{p_x}{\Omega_o m_o} \ ,
\end{aligned} \tag{10}$$

which are, respectively, the transverse momentum, the azimuthal phase angle relative to a fixed cyclotron helix, the parallel momentum, and the

x and y locations of the guiding center, defined as functions of the Cartesian components of position (x,y,z) and momentum (p_x, p_y, p_z). The nonrelativistic cyclotron frequency is $\Omega_0 = eB_0/m_0c$. Considering Eq. (10) as a transformation from Cartesian to constant-of-motion phase space, that is, defining $g^{(0)} = f^{(0)}$ ang $g^{(1)} = f^{(1)}$, where $g^{(0)}$ and $g^{(1)}$ are functions of the variables defined in Eq. (10) as well as z and t, the Vlasov equations can be written as

$$\left(\frac{\partial}{\partial t} + \frac{p_{\parallel}}{\gamma m_0}\frac{\partial}{\partial z}\right) g^{(1)} = e\left[\delta\underset{\sim}{E} + \frac{1}{\gamma m_0 c}\underset{\sim}{p} \times \delta\underset{\sim}{B}\right]\cdot\frac{\partial}{\partial \underset{\sim}{p}} g^{(0)} \quad . \tag{11}$$

Here the unperturbed distribution function is assumed independent of θ, x_g and y_g. The relativistic factor γ is defined as $\gamma^2 = 1 + (p_{\parallel}^2 + p_{\perp}^2)/(m_0c)^2$.

Using Eqs. (3) and (10) and introducing the expansion

$$g^{(1)} = \tilde{g}^{(1)}e^{-i\omega t} + c.c \ , \tag{12}$$

in Eq. (11), the first order linear homogeneous differential equation for $\tilde{g}^{(1)}$ can be integrated, yielding

$$\begin{aligned}\tilde{g}^{(1)} = \frac{1}{4} eA_0 \frac{\gamma m_0}{p_{\parallel}} \exp\left[i\frac{\gamma m_0\omega}{p_{\parallel}} z\right] \\ \times \left\{(1+\varepsilon)e^{i\theta}\left[\frac{e^{i\xi_{1+}z}-1}{i\xi_{1+}} D_+ - \frac{e^{i\xi_{1-}z}-1}{i\xi_{1-}} D_-\right]\right. \\ \left. - (1-\varepsilon)e^{-i\theta}\left[\frac{e^{-i\xi_{2-}z}-1}{i\xi_{2-}} D_+ - \frac{e^{-i\xi_{2+}z}-1}{i\xi_{2+}} D_-\right]\right\} g^{(0)} \ .\end{aligned} \tag{13}$$

The differential operators, D_+ and D_-, acting on $g^{(0)}$, and the relative wavenumbers, $\xi_{1\pm}$ and $\xi_{2\pm}$, are

$$D_{\pm} = \frac{\omega}{c}\frac{\partial}{\partial p_{\perp}} \pm \frac{k}{\gamma m_o c}\left(p_{\perp}\frac{\partial}{\partial p_{\parallel}} - p_{\parallel}\frac{\partial}{\partial p_{\perp}}\right)$$

$$\xi_{1\pm} = \pm k + \frac{(\Omega_o - \gamma\omega)m_o}{p_{\parallel}} \tag{14}$$

$$\xi_{2\pm} = \pm k + \frac{(\Omega_o + \gamma\omega)m_o}{p_{\parallel}} \quad .$$

The constant of integration in Eq. (13) is such that $\tilde{g}^{(1)} = 0$ at $z=0$, corresponding to an unperturbed entering beam.

The perturbed distribution function, obtained in Eq. (13), can be used to evaluate the Fourier component of the current density,

$$\tilde{\underset{\sim}{J}} = -\frac{e}{m_o}\int \frac{\underset{\sim}{p}}{\gamma}\,\tilde{g}^{(1)}\,d\underset{\sim}{p} \quad . \tag{15}$$

Performing the integration over θ in Eq. (15) gives

$$\tilde{\underset{\sim}{J}} = -\frac{1}{8}e^2 A_o n_o \int dp_{\perp}\,dp_{\parallel}\,\frac{p_{\perp}^2}{p_{\parallel}}\exp\left[i\,\frac{\gamma m_o\omega}{p_{\parallel}}\,z\right]$$

$$\times\left\{(\hat{\underset{\sim}{e}}_x + i\hat{\underset{\sim}{e}}_y)\exp\left[-i\,\frac{\Omega_o m_o}{p_{\parallel}}\,z\right](1+\varepsilon)\left[\frac{e^{i\xi_{1+}z}-1}{i\xi_{1+}}D_+ - \frac{e^{i\xi_{1-}z}-1}{i\xi_{1-}}D_-\right]\right.$$

$$\left. - (\hat{\underset{\sim}{e}}_x - i\hat{\underset{\sim}{e}}_y)\exp\left[i\,\frac{\Omega_o m_o}{p_{\parallel}}\,z\right](1-\varepsilon)\left[\frac{e^{-i\xi_{2-}z}-1}{i\xi_{2-}}D_+ - \frac{e^{-i\xi_{2+}z}-1}{i\xi_{2+}}D_-\right]\right\}g_o \; . \tag{16}$$

The beam density n_o has been extracted for convenience from the distribution function, by defining $n_o g_o = 2\pi g^{(0)}$, where g_o is normalized to $\int dp_{\perp}\int dp_{\parallel}p_{\perp}g_o = 1$. Finally, multiplying $\tilde{\underset{\sim}{J}}$ by $\sin(kz)$ and integrating over the length of interaction, yields the driving term required in Eq. (6),

$$\int_0^L 4\pi c\, \tilde{\underset{\sim}{J}} \sin(kz)\, dz$$

$$= i\, \frac{\pi}{4}\, e^2 A_0 n_0 c \int dp_\perp dp_{//}\, \frac{p_\perp^2}{p_{//}}$$

$$\times \Bigg\{ (\hat{\underset{\sim}{e}}_x + i\hat{\underset{\sim}{e}}_y)\,(1+\varepsilon) \Bigg[\left(\frac{e^{-i\xi_{1-}L} - 1}{i\xi_{1-}} - L - \frac{e^{-i\xi_{1+}L} - 1}{i\xi_{1+}} \right) \frac{1}{i\xi_{1+}} D_+$$

$$- \left(L + \frac{e^{-i\xi_{1-}L} - 1}{i\xi_{1-}} - \frac{e^{-i\xi_{1+}L} - 1}{i\xi_{1+}} \right) \frac{1}{i\xi_{1-}} D_- \Bigg]$$

$$- (\hat{\underset{\sim}{e}}_x - i\hat{\underset{\sim}{e}}_y)\,(1-\varepsilon) \Bigg[\left(- \frac{e^{i\xi_{2+}L} - 1}{i\xi_{2+}} - L + \frac{e^{i\xi_{2-}L} - 1}{i\xi_{2-}} \right) \frac{1}{i\xi_{2-}} D_+$$

$$- \left(L - \frac{e^{i\xi_{2+}L} - 1}{i\xi_{2+}} + \frac{e^{i\xi_{2-}L} - 1}{i\xi_{2-}} \right) \frac{1}{i\xi_{2+}} D_- \Bigg] \Bigg\} g_0 \,, \tag{17}$$

where the boundary condition $\sin(kL) = 0$ has been used to eliminate terms similar to $\exp\left[i(\xi_{1+} - \xi_{1-})L\right]$.

Equating Eqs. (6) and (17) yields a consistency condition between ω_R, Γ and ε. This is the linear dispersion relation, which includes the positive and negative electron cyclotron interaction with both the forward and backward traveling waves. However, in general only one of these interactions is resonant, which we take throughout the remainder of this paper to be with the forward wave.[30] Defining

$$\xi = \xi_{1+} = k + \frac{(\Omega_0 - \gamma\omega)m_0}{p_{//}} \,,$$

$$\mu = \frac{1}{2}\, \xi L \,, \tag{18}$$

one obtains from Eq. (17),

$$\int_0^L 4\pi c\, \tilde{\underset{\sim}{J}} \sin(kz)dz$$

$$= i\,\frac{\pi}{4}\, e^2 A_o n_o c \int dp_\perp dp_{\parallel} \frac{p_\perp^2}{p_{\parallel}} (\hat{\underset{\sim}{e}}_x + i\hat{\underset{\sim}{e}}_y)\ (1+\varepsilon) \left[\frac{iL}{\xi} + \frac{e^{-i\xi L}-1}{\xi^2}\right] D_+ g_o . \quad (19)$$

Comparing this equation with Eq. (6), it is seen immediately that consistency requires that $\varepsilon=1$, that is, only a circular polarization is compatible with the interaction. The dispersion relation now becomes

$$(\omega_R^2 - k^2c^2) + i\omega_R(2\Gamma + \frac{\omega_R}{Q})$$

$$= \frac{1}{16}\, m_o L c \omega_{b_o}^2 \int dp_\perp dp_{\parallel} \frac{p_\perp^2}{p_{\parallel}} \left[\frac{2\mu - \sin 2\mu}{\mu^2} + i2\,\frac{\sin^2\mu}{\mu^2}\right] D_+ g_o\ , \quad (20)$$

where $\omega_{bo}^2 = 4\pi e^2 n_o/m_o$ and μ is a complex quantity, defined in Eq. (18) and depending on $\omega = \omega_R + i\Gamma$.

In a number of interesting special cases only the real part μ_R of μ is of significance. These cases are: (i) the (linear) steady state, $\Gamma = 0$, (ii) the conditions just above threshold, $\Gamma \to 0$, and (iii) when the beam is sufficiently weak, so that the imaginary part of μ is negligible. In such cases, separate equations can be obtained for the frequency and growth rate,

$$\omega_R^2 - (kc)^2 = \frac{1}{4}\, m_o L c \omega_{bo}^2 \int dp_\perp dp_{\parallel} \frac{p_\perp^2}{p_{\parallel}} \frac{2\mu_R - \sin 2\mu_R}{(2\mu_R)^2} D_+ g_o\ ,$$

$$\omega_R(2\Gamma + \frac{\omega_R}{Q}) = \frac{1}{8}\, m_o L c \omega_{bo}^2 \int dp_\perp dp_{\parallel} \frac{p_\perp^2}{p_{\parallel}} \frac{\sin^2\mu_R}{\mu_R^2} D_+ g_o\ . \quad (21)$$

Finally, for the special case of a monoenergetic beam, $g_o = \delta(p_\perp - p_{\perp o})\,\delta(p_{\parallel} - p_{\parallel o})/p_{\perp o}$, integration over $p_\perp$ and $p_{\parallel}$ gives

$$\left.\begin{array}{l}\dfrac{1-n^2}{2}\\[2ex]\dfrac{2\Gamma}{\omega_R}+\dfrac{1}{Q}\end{array}\right\} = \frac{1}{8}\left(\frac{\beta_{\perp o}}{\beta_{\parallel o}}\right)^2 \frac{\omega_{bo}^2}{\gamma_o}\,\frac{L}{\omega_R c}\,D_\mu \left\{\begin{array}{l}R_n(\mu_R)\ ,\\[2ex] R_Q(\mu_R)\ ,\end{array}\right. \tag{22}$$

where the refractive index, $n = kc/\omega_R$, has been introduced, the quantity μ_R is obtained from Eq. (18) in terms of the beam quantities γ_o and $p_{\parallel o}$ and the dimensionless velocities $\beta_{\parallel o} = p_{\parallel o}/\gamma_o m_o c$ and $\beta_{\perp o} = p_{\perp o}/\gamma_o m_o c$ were used. The operator D_μ and the functions R_n and R_Q are

$$D_\mu = \left[n - 2\,\frac{\beta_{\parallel o}(1-n\beta_{\parallel o})}{\beta_{\perp o}^2}\right] + \left[\frac{1-n^2}{2}\,\frac{\omega_R L}{c} + n\mu_R\right]\frac{d}{d\mu_R}\ ,$$

$$R_n(\mu) = \frac{2\mu - \sin 2\mu}{(2\mu)^2}\ , \tag{23}$$

$$R_Q(\mu) = \left(\frac{\sin\mu}{\mu}\right)^2\ .$$

To complete the formalism we note that for the fields of Eq. (3) the total steady state field energy inside the interaction region, L, is given by $\int_0^L u\,dz = (\omega_R A_o/2c)^2\ L\ (1 + n^2)/\pi$, hence the efficiency of converting kinetic energy to radiation energy, per unit time, is

$$\eta_\ell = \frac{1 + n^2}{2\gamma_o(\gamma_o-1)}\ \frac{\beta_{\perp o}^2}{\beta_{\parallel o}^3}\left(\frac{eA_o}{2mc^2}\right)^2\left(\frac{\omega_R L}{c}\right)^2 D_\mu R_Q\ . \tag{24}$$

We have thus completed the linear analysis of the interaction. The results are represented by Eqs. (22) and (24) for a monoenergetic beam and weak (or vanishing) growth-rate, as well as the general case given by Eq. (20). Let us consider now the significance of these equations,

in the limiting cases $n \to 0$ and $n \to 1$. The first of these cases, $n \to 0$, corresponds to the gyrotron mechanism. Referring to Eq. (24), the efficiency of the oscillator is proportional to the quantity

$$D_\mu R_Q = -2\frac{\beta_{\parallel o}}{\beta_{\perp o}^2}\left(\frac{\sin\mu_R}{\mu_R}\right)^2 + \frac{1}{2}\frac{\omega_R L}{c}\frac{d}{d\mu_R}\left(\frac{\sin\mu_R}{\mu_R}\right)^2 \quad . \tag{25}$$

The first term in the above expression is always negative, and its stabilizing effects are reduced if the ratio $\beta_{\perp o}^2/\beta^2{}_o$ is large. If this ratio is large enough for this term to be omitted, a positive energy conversion can be obtained if the derivative $dR_Q/d\mu_R$ is positive. This occurs in a number of intervals in the domain of μ_R, the most prominent of which is $-\pi < \mu_R < 0$, and the maximum of $dR_Q/d\mu_R = 0.54$ is attained at $\mu_R = -1.3$. Such negative values for μ_R correspond to $\omega_R > \Omega_o/\gamma_o$, hence the wave frequency must exceed the relativistic electron gyrofrequency.

Let us now turn our attention to the interaction with luminous waves, $n \to 1$. In this case, the efficiency of the resonator, referring to Eq. (24), is proportional to

$$D_\mu R_Q = \left[1 - 2\frac{\beta_{\parallel o}(1-\beta_{\parallel o})}{\beta_{\perp o}^2}\right]\left(\frac{\sin\mu_R}{\mu_R}\right)^2 + \mu_R\frac{d}{d\mu_R}\left(\frac{\sin\mu_R}{\mu_R}\right)^2 \quad . \tag{26}$$

This function is plotted in Fig. (2) for $\beta_{\parallel o} = 0.1$ and (a) $\beta_{\perp o} = 0.7$, (b) $\beta_{\perp o} = 0.425$, and (c) $\beta_{\perp o} = 0.35$. A number of interesting features can be observed in Eq. (26). First it is noted that $D_\mu R_Q$ (i.e., η_ℓ) is an even function of μ_R, therefore, contrary to the gyrotron mechanism, the interaction with luminous waves does not depend on the sign of the frequency mismatch, $\Delta\omega_o = \omega_R - \Omega_o/\gamma_o - kv_{\parallel o} = -2\mu_R v_{\parallel o}/L$. Instability occurs if either of two conditions are satisfied. The first is

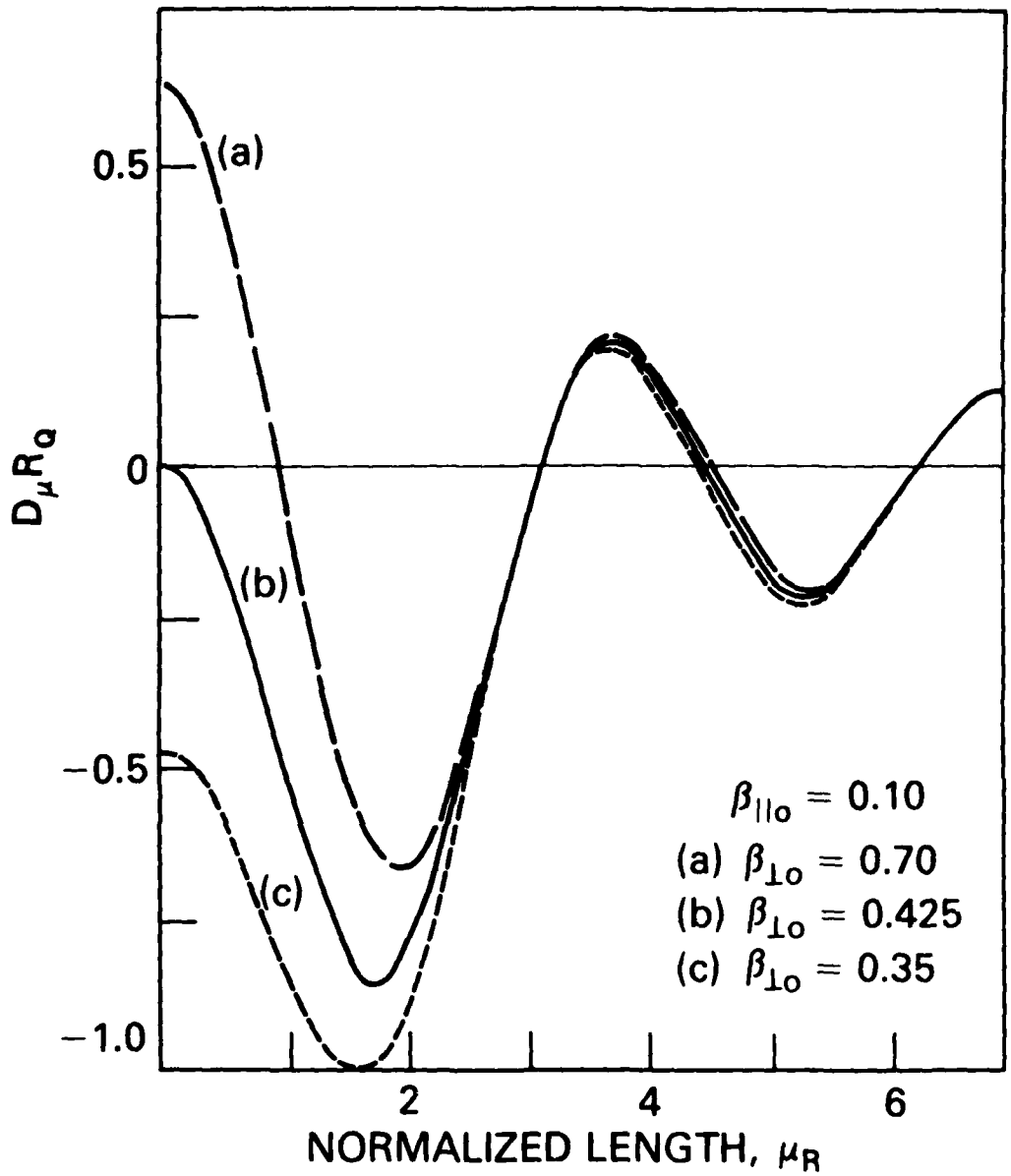

Fig. 2 — The function $D_\mu R_Q(\mu_R)$, which is proportional to the linear efficiency, versus μ_R, which is proportional to the resonator length, for n=1, $\beta_{||o} = 0.1$ and (a) $\beta_{\perp o} = 0.70$, (b) $\beta_{\perp o} = 0.425$, and (c) $\beta_{\perp o} = 0.35$.

$$\beta_{\perp o}^2 > 2\beta_{\parallel o}(1 - \beta_{\parallel o}) , \tag{27}$$

and $\mu_R = 0$. If Eq. (27) is satisfied, the first term in Eq. (26) is positive, while the second term vanishes. Thus, contrary to the gyrotron mechanism, a positive efficiency can occur for $\Delta\omega = 0$, provided that Eq. (27) is satisfied. If Eq. (27) is well satisfied, the first term dominates up to the point $|\mu_R| = 1.166$, where $\tan\mu_R = 2\,\mu_R$ and therefore $-\,\mu_R\, dR_Q/d\mu_R = R_Q$. Additional regions of instability occur when the second term is positive, provided that Eq. (27) is not too strongly violated. These regions cover the intervals $j\pi < |\mu_R| < a_j - 1/a_j$, where $a_j = (2j+1)\pi/2$, $j=1,2,3...$, and the upper limit is a good approximation to the solution of $\tan\mu_R = \mu_R$. In these regions, $\mu_R\, dR_Q/d\mu_R$ reaches the maximum values $1/(1 + b_j)$ at $|\mu_R| = b_j - 1/(\sqrt{2}\, b_j)$, where $b_j = (4j + 1)\pi/4$, and j is a positive integer.

III. NONLINEAR THEORY

The linear analysis established that the cyclotron interaction with plane waves results in instability, even for luminous waves, $n \to 1$. In this section the nonlinear equations of motion are obtained, both on the fast and slow spatial scales. These equations are investigated and constants of the motion are obtained. The application of these invariants permits the analytical study of the conditions for energy depletion, the trajectories in phase space and the exact scaling relations for the efficiency. A single first-order differential equation is found to be sufficient to describe the evolution of the particles.

The nonlinear equations of motion are studied under the action of a uniform axial magnetic field, $\underset{\sim}{B}_0 = B_0 \hat{\underset{\sim}{e}}_z$, specified by its nonrelativistic electron gyrofrequency, $\Omega_0 = eB_0/mc$, and a steady state wave, whose vector potential is

$$\underset{\sim}{A} = A_0 \left[\hat{\underset{\sim}{e}}_x \sin(kz - \omega t + \phi_0) + \varepsilon \, \hat{\underset{\sim}{e}}_y \cos(kz - \omega t + \phi_0) \right] . \qquad (28)$$

Only the forward wave is included in Eq. (28). Adding to Eq. (28) a similar expression, with $k \to -k$ and $\phi_0 \to \phi_0 + \pi$, recovers Eq. (2). However, the backward wave has been omitted, since resonance with the forward component is assumed.

Although the natural independent variable for particle motion is time, it is convenient for oscillator configurations to adopt a Lagrangian representation, expressing the equations of motion in terms of the axial distance z. Since $dt = dz/v_z$, the phase of the wave as a function of z is given by

$$\psi(z) = k \int_0^z \left(1 - \frac{1}{n\beta_z(z')}\right) dz' + \psi_0 \tag{29}$$

where $\beta_z = v_z/c$. The equations of motion become

$$\frac{d}{dz}(\gamma\beta_x) = A_0 \cos\psi \frac{d\psi}{dz} - \frac{\Omega_0}{c} \frac{\beta_y}{\beta_z} ,$$

$$\frac{d}{dz}(\gamma\beta_y) = -\varepsilon A_0 \sin\psi \frac{d\psi}{dz} + \frac{\Omega_0}{c} \frac{\beta_x}{\beta_z} ,$$

$$\frac{d}{dz}(\gamma\beta_z) = -k A_0 \left(\frac{\beta_x}{\beta_z} \cos\psi - \varepsilon \frac{\beta_y}{\beta_z} \sin\psi\right) , \tag{30}$$

$$\frac{d}{dz}\gamma = -k \frac{A_0}{n} \left(\frac{\beta_x}{\beta_z} \cos\psi - \varepsilon \frac{\beta_y}{\beta_z} \sin\psi\right),$$

$$\frac{d}{dz} x = \frac{\beta_x}{\beta_z} , \qquad \frac{d}{dz} y = \frac{\beta_y}{\beta_x} ,$$

where $A_0 = eA_0/mc^2$, $\beta_x = v_x/c$, $\beta_y = v_y/c$ and $\gamma^2 = (1 - \beta_x^2 - \beta_y^2 - \beta_z^2)^{-1}$. Note that the first four of Eq. (30) are interrelated by the definition of γ. In addition, the equations for x and y can be integrated, in conjunction with the equations for $\gamma\beta_y$ and $\gamma\beta_x$, respectively, to yield the constants of the motion

$$I_x = \gamma\beta_x - A_0 \sin\psi + \frac{\Omega_0}{c} y ,$$

$$I_y = \gamma\beta_y - \varepsilon A_0 \cos\psi - \frac{\Omega_0}{c} x .$$

These integrals can be used to assess the assumption of transverse uniformity implied by Eq. (28).

An additional invariant can be obtained from Eq. (30) by noting the equations for $\gamma\beta_z$ and γ. This invariant[30] is

$$I_1 = \gamma(n - \beta_z) \quad , \tag{31}$$

and its invariance is associated with the plane wave nature of the fields. When n=0, this invariant describes the conservation of axial momentum in the cut-off frame of the gyrotron.[12] If $n > 1$, I_1 is proportional to the conserved particle energy in the wave frame.[33,34] The significance of this invariant is that it indicates the possibility of complete energy depletion, $\gamma=1$, if the initial particle properties are such that $I_1 = n$. Denoting these initial properties with a subscript zero, the necessary condition for complete energy depletion is

$$\gamma_o = \frac{n}{n-\beta_{zo}} \quad . \tag{32}$$

Introducing the definition of γ_o, Eq. (32) can be written as

$$\beta_{\perp o}^2 = 2\,\frac{\beta_{zo}}{n}\left(1 - \beta_{zo}\,\frac{n^2+1}{2n}\right) \quad , \tag{33}$$

where $\beta_{\perp o}^2 = \beta_{xo}^2 + \beta_{yo}^2$. An interesting observation is that when n=1, Eq. (33) reproduces the condition for the vanishing of the first term in the linear dispersion relation (see Eq. (26)). It should be noted that Eq. (32) or (33) represents only a necessary condition for complete energy depletion. The sufficient condition depends on whether the state of complete energy depletion is accessible by the particles. We will return to this point later.

The introduction of the invariants reduces the system of Eq. (30) formally to two coupled integro-differential equations for $\gamma\beta_x$ and $\gamma\beta_y$. Following the usual procedure,[7] we define

$$\beta_x = \beta_\perp \sin(\psi + \chi) \quad ,$$
$$\beta_y = \beta_\perp \cos(\psi + \chi) \quad , \tag{34}$$

where $\beta_\perp$, ψ and χ are functions of z varying slowly over a cyclotron period. Substituting Eq. (34) into Eq. (30) results in trigonometric functions with arguments χ and $2\psi + \chi$. The $2\psi + \chi$ terms phase-mix in a few wavelengths, hence the slow spatial scale equations are

$$\frac{d}{dz}(\gamma\beta_\perp) = \frac{1+\varepsilon}{2} k \left(1 - \frac{1}{n\beta_z}\right) A_0 \sin\chi \quad ,$$

$$\frac{d}{dz}(\gamma\beta_z) = -\frac{1+\varepsilon}{2} k \frac{\beta_\perp}{\beta_z} A_0 \sin\chi \quad , \tag{35}$$

$$\frac{d}{dz}\chi = -k\left[1 - \frac{1}{n\beta_z}\left(1 - \frac{\Omega_0}{\omega\gamma}\right)\right] + \frac{1+\varepsilon}{2} k \frac{1}{\gamma\beta_\perp}\left(1 - \frac{1}{n\beta_z}\right) A_0 \cos\chi \quad ,$$

$$\frac{d}{dz}\gamma = -\frac{1+\varepsilon}{2} k \frac{\beta_\perp}{n\beta_z} A_0 \sin\chi \quad .$$

The above equations are interrelated by the definition of γ and the invariance of I_1. In addition, Eq. (35) possesses and additional invariant, given by

$$I_2 = (\gamma\beta_\perp)^2 - (\gamma\beta_\perp)(1+\varepsilon)A_0 \cos\chi - 2\frac{\Omega_0}{kc} n\gamma \quad . \tag{36}$$

It can be seen that when n=0, ε=0 and $\beta_z \to 0$, the combination $I_2 + I_1^2 + 1 + (\Omega_0/\omega)^2$ gives the corresponding gyrotron type invariant in the cut-off frame.[12] Also, when $n > 1$, then I_2 transforms in the wave frame to the corresponding second invariant.[33,34] Furthermore, using the fast length scale Eq. (30), the derivative of I_2 is

$$\frac{dI_2}{dz} = -(1-\varepsilon)\, kA_0 \left\{ \left[1 - \frac{1}{n\beta_z}\left(1 - \frac{\Omega_0}{\omega\gamma}\right)\right] \gamma\beta_\perp \sin(2\psi + \chi) + \left(1 - \frac{1}{n\beta_z}\right) \frac{1+\varepsilon}{2} A_0 \sin 2\psi \right\} . \tag{37}$$

Hence I_2 is invariant also on the fast length scale, provided ε=1.

The determination of the two invariants, I_1 and I_2, allows us to study the trajectories in phase space. The appropriate coordinates for the two-dimensional representation are χ and γ. Using the definition of γ and the invariance of I_1 and I_2 to eliminate β_z and $\beta_\perp$ in terms of γ and χ (and the initial conditions, denoted by subscript zero), we find that

$$\cos\chi = \frac{(1-n^2)\,(\gamma-\gamma_0)^2 + 2(\Delta\omega_0/\omega)\,\gamma_0\,(\gamma-\gamma_0) + (1+\varepsilon)\,A_0\gamma_0\,\beta_{\perp 0}\cos\chi_0}{(1+\varepsilon)\,A_0\left[(1-n^2)\,(\gamma-\gamma_0)^2 + 2(1-n\beta_{z0})\,\gamma_0\,(\gamma-\gamma_0) + (\gamma_0\beta_{\perp 0})^2\right]^{1/2}} , \tag{38}$$

where $\Delta\omega_0 = \omega - \Omega_0/\gamma_0 - kv_{z0}$.

We are primarily interested in the case of luminous waves, n=1. In this case, Eq. (38) takes on a rather simple form. The resultant equation is

$$qC_w - q^{1/2}\cos\chi = \text{const} , \tag{39}$$

where C_w is a constant proportional to the ratio of the initial frequency mismatch and the wave amplitude,

$$C_w = \frac{\gamma_0\beta_{\perp 0}}{1-\beta_{z0}} \quad \frac{\omega - kv_{z0} - \Omega_0/\gamma_0}{\omega(1+\varepsilon)A_0} \quad , \tag{40}$$

and q is a linear function of γ,

$$q = 2\,\frac{1-\beta_{z0}}{\gamma_0\beta_{\perp 0}^2}\,(\gamma-\gamma_0) + 1. \tag{41}$$

It can be seen that q=1 corresponds to the initial condition, $\gamma=\gamma_0$, hence the constant in Eq. (39) is equal to $C_w - \cos\chi_0$. In addition, depletion of the perpendicular or of the parallel energy, correspond to q=0 and $q=C_d$ respectively, where

$$C_d = 1 - \frac{2\beta_{z0}(1-\beta_{z0})}{\beta_{\perp 0}^2} \quad , \tag{42}$$

is a constant characterizing the anisotropy of the distribution. When $C_d=0$, complete depletion of the energy is possible, see Eq. (33).

For a positive frequency mismatch, that is, when $C_w > 0$, the phase space trajectories, obtained from Eq. (39), are shown schematically in Fig. (3). The arrows indicate the direction of particle motion. Both open and closed trajectories are possible in principle. The separatrix between these two families of curves is shown by the broken bell-shaped curve, described by the equation $qC_w^2 - \cos^2\chi = 0$ and defined only in the interval $|\chi| \leq \pi/2$. The largest value of q on the separatrix is at $\chi=0$, $q=C_w^{-2}$. The vortex, or O-point, of the closed trajectories is at $\chi=0$, $q = (2C_w)^{-2}$.

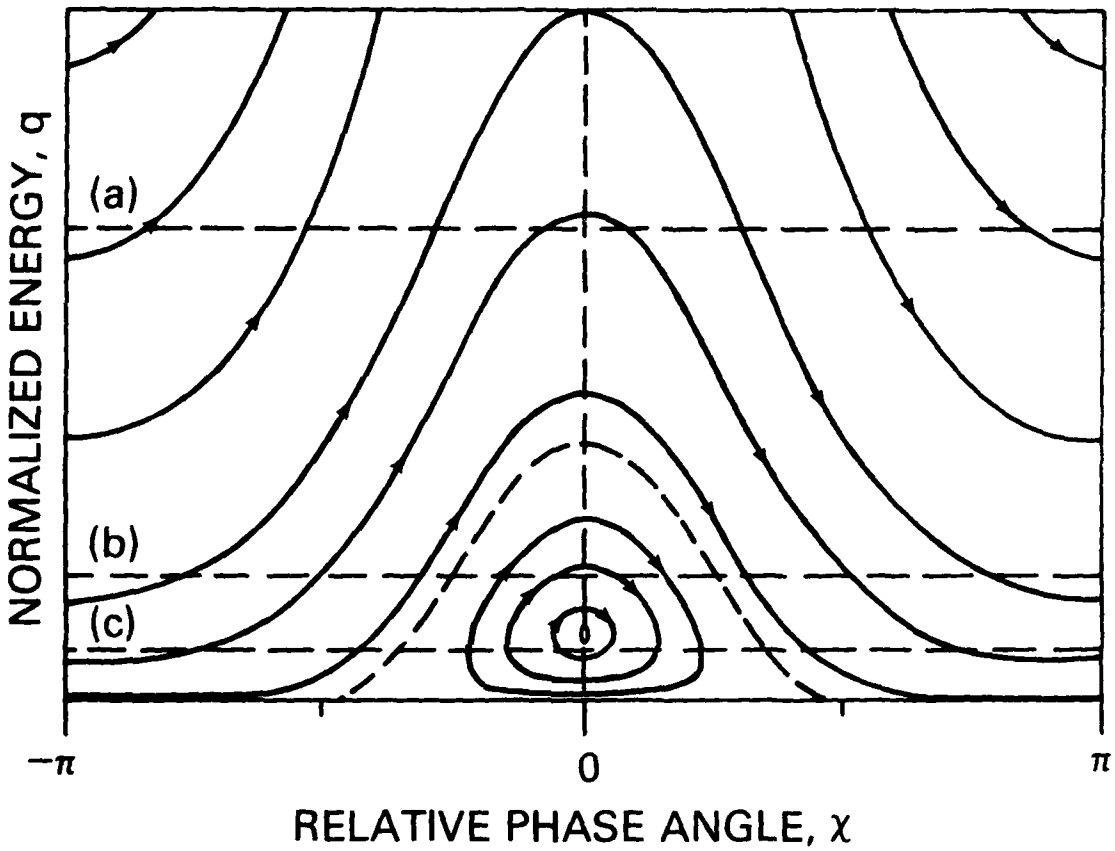

Fig. 3 — Trajectories in phase space coordinates q, χ. The dashed curve is the separatrix. The dashed straight lines give the initial values, q=1, for (a) $C_w > 1$, (b) $0.5 < C_w < 1$, and (c) $0 < C_w < 0.5$.

For the curves in Fig. (3) to represent actual electron trajectories, they must intersect the initial condition line, $q_0=1$. The location of this line can be obtained in relation to the value of C_w. If $C_w > 1$, then the peak of the separatrix lies below the line $q_0=1$ (line (a)), and all particles are untrapped. Trapped particles exist if $C_w < 1$, but always more than half of the initial phase angles χ_0 correspond to untrapped particles. Lines (b) and (c) in Fig. (3) describe the initial conditions, $q_0=1$, if $0.5 < C_w < 1$ and $0 < C_w < 0.5$, that is, above and below the vortex, respectively.

When $C_w < 0$, the phase space trajectories are obtained from those in Fig. (3) by a reflection about the line $\chi=\pi/2$. The trajectories for $C_w > 0$ and $C_w < 0$ are shown in Figs. 4(a) and (b). Because of this symmetry, any particle, trapped or untrapped, in Fig. 4(a) has a corresponding particle in Fig. 4(b), which executes identical changes in q (or γ). This recovers and extends to the nonlinear regime the linear result that the evolution is independent of the sign of the frequency mismatch (or C_w). The phase plot in Fig. 4(c) corresponds to exact synchronism, $C_w=0$. In this case the separatrix reduces to the lines $\chi=\pi/2$ and $\chi=-\pi/2$ and all particles are semi-trapped. In this case the relative phase χ is bounded, while the energy, or q, is bounded only from below. Whether the initial evolution in this case corresponds to net particle energy loss or gain depends on whether $C_d > 0$ or $C_d < 0$, as has been shown in linear theory. However, it is clear from Fig. 4(c) that eventually all particles, regardless of their initial phase, will gain energy and will be tightly bunched in χ (but not in energy), about $\chi=-\pi/2$. Accordingly, this configuration can be the basis for a particle

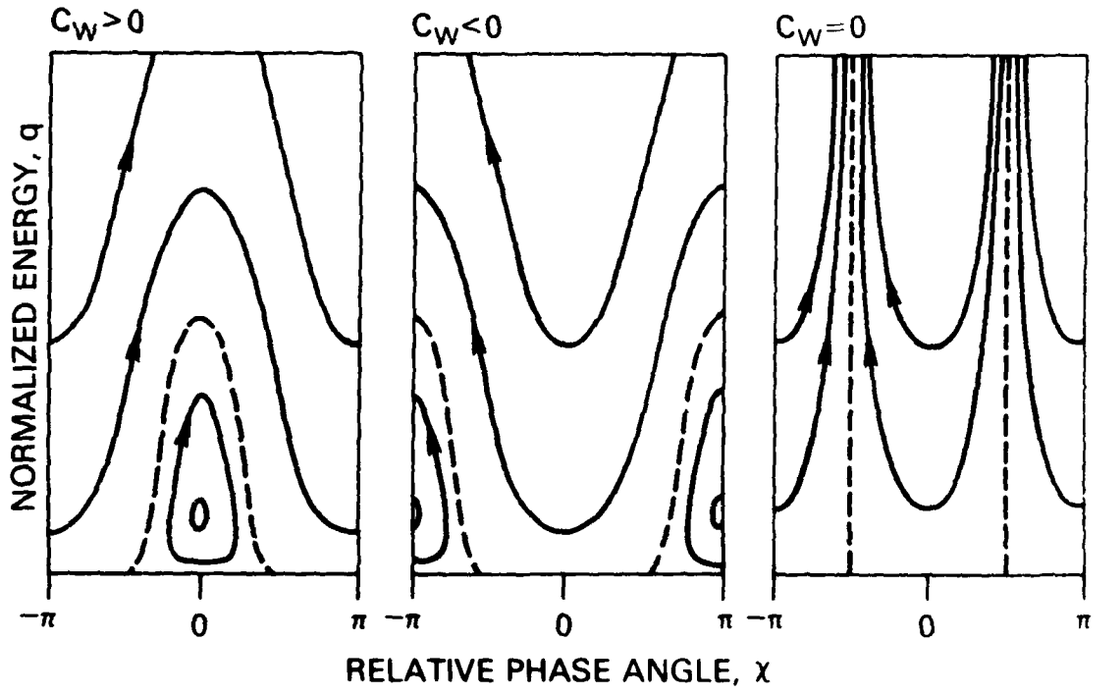

Fig. 4 — Comparison of phase space trajectories when (a) $C_w > 0$, (b) $C_w < 0$, and (c) $C_w = 0$.

accelerator. The details of such an application are currently under study and will be discussed in a separate publication.

The determination of the two invariants, I_1 and I_2, which connect the three independent momentum components, makes possible the description of the electron evolution in terms of only one quantity, say q (i.e., the energy). When the index of refraction is unity, i.e., $n=1$, the corresponding differential equation is

$$\frac{dq}{d\zeta} = - \operatorname{sgn}(\sin\chi) \frac{\left[q - (qC_w - C_w + \cos\chi_0)^2\right]^{\frac{1}{2}}}{q-C_d} \tag{43}$$

where sgn is the sign function and the reduced length ζ is defined as

$$\zeta = \frac{2(1+\varepsilon)A}{\gamma_0\beta_{\perp 0}} \left(\frac{1-\beta_{z0}}{\beta_{\perp 0}}\right)^2 k(z-z_0) \ . \tag{44}$$

It can be seen that Eq. (43) is immediately integrable. The inversion of the resulting expression is straightforward only when $C_w=0$, $C_d < 0$. This case is, however, uninteresting, since it corresponds to energy gain by the electrons.

In spite of the difficulties associated with the inversion of the integral of Eq. (43), useful information can still be obtained. It is noted that the solution of Eq. (43) has the form

$$q = q(\zeta_{max}; \chi_0, C_w, C_d) \quad , \tag{45}$$

where ζ_{max} is the value of ζ corresponding to the length L of the interaction region in Eq. (44). In our Lagrangian representation, the efficiency is given by $\eta = -\langle\gamma-\gamma_0\rangle / (\gamma_0-1)$, hence

$$\eta(\zeta_{max}, C_w, C_d, C_\eta) = C_\eta \, (1-\langle q \rangle \, , \tag{46}$$

where the angular brackets denote an ensemble average over χ_o and the coefficient C_η is defined by

$$C_\eta = \frac{\gamma_o \beta_{\perp o}^2}{2(\gamma_o - 1)\,(1-\beta_{zo})} \quad . \tag{47}$$

The efficiency, therefore, does not depend on the seven parameters k, A, ε, L, β_{zo}, $\beta_{\perp o}$, Ω_o arbitrarily but only on ζ_{max}, C_w, C_d and C_η. Further simplifications arise by the fact that C_η is just a multiplier of the efficiency expression. Large values of C_η are possible for a wide range of beam properties, as can be seen in Fig. (5). In this figure contour plots, C_η = const, are presented. In addition, Fig. (6) presents contour plots of C_d = const.

Before proceeding with the presentation of the results for the non-linear efficiency, it is worthwhile to rewrite the linear efficiency, Eq. (24), in terms of the variables defined above. We use the definitions of C_d, C_w, C_η and note from the definition of ζ that it is related to μ_o by $C_w \zeta_{max} = -\,2(1-C_d)\mu_o$, where μ_o is defined in Eq. (18) in terms of the initial values. Then from Eq. (24) the expression for the linear efficiency is obtained,

$$\eta_\ell = \frac{C_\eta}{C_w^2\,(1-C_d)}\,\mu_o^2\,\left(C_d + \mu_o \frac{d}{d\mu_o}\right)\left(\frac{\sin\mu_o}{\mu_o}\right)^2 \quad . \tag{48}$$

This expression has all the features expected from Eq. (46), since it involves a dependence on ζ_{max} (through μ_o), as well as C_w, C_d and C_η.

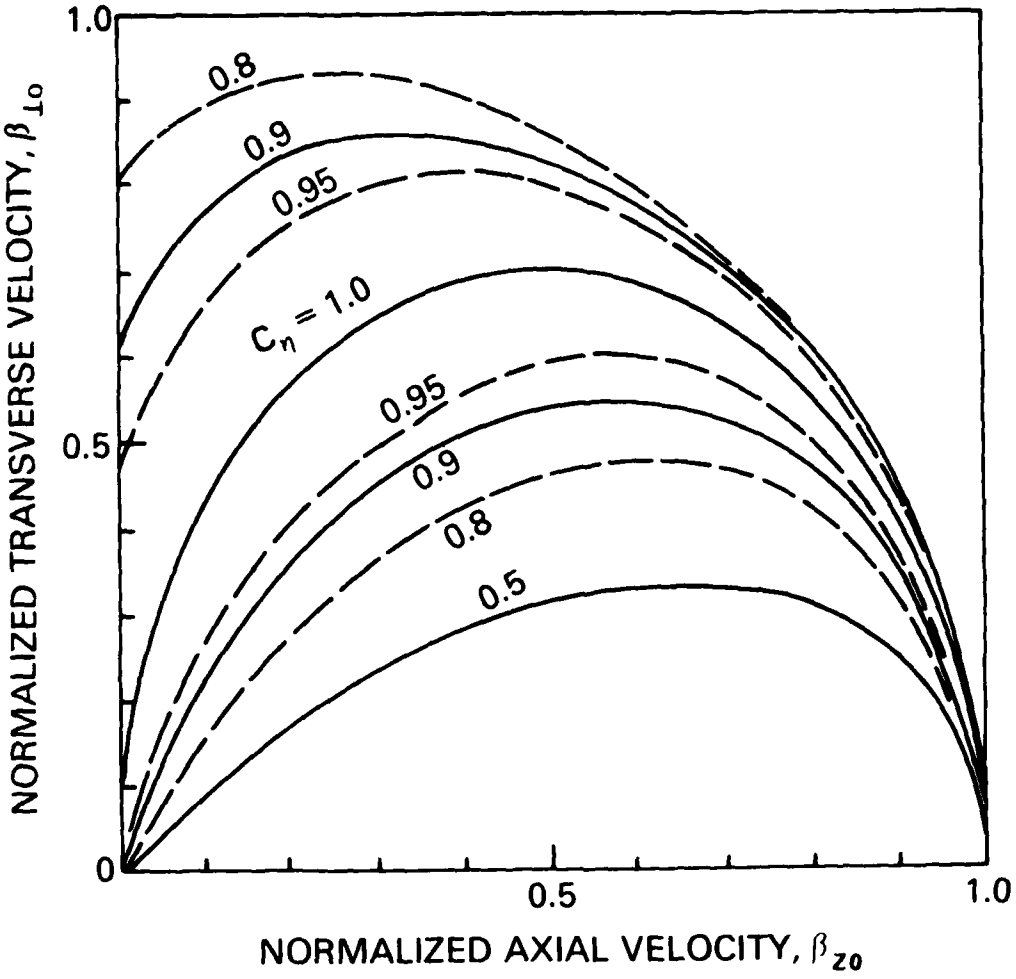

Fig. 5 — Contour plots for the efficiency coefficient C_η vs. β_{zo} $\beta_{\perp o}$, the normalized transverse and axial electron velocities.

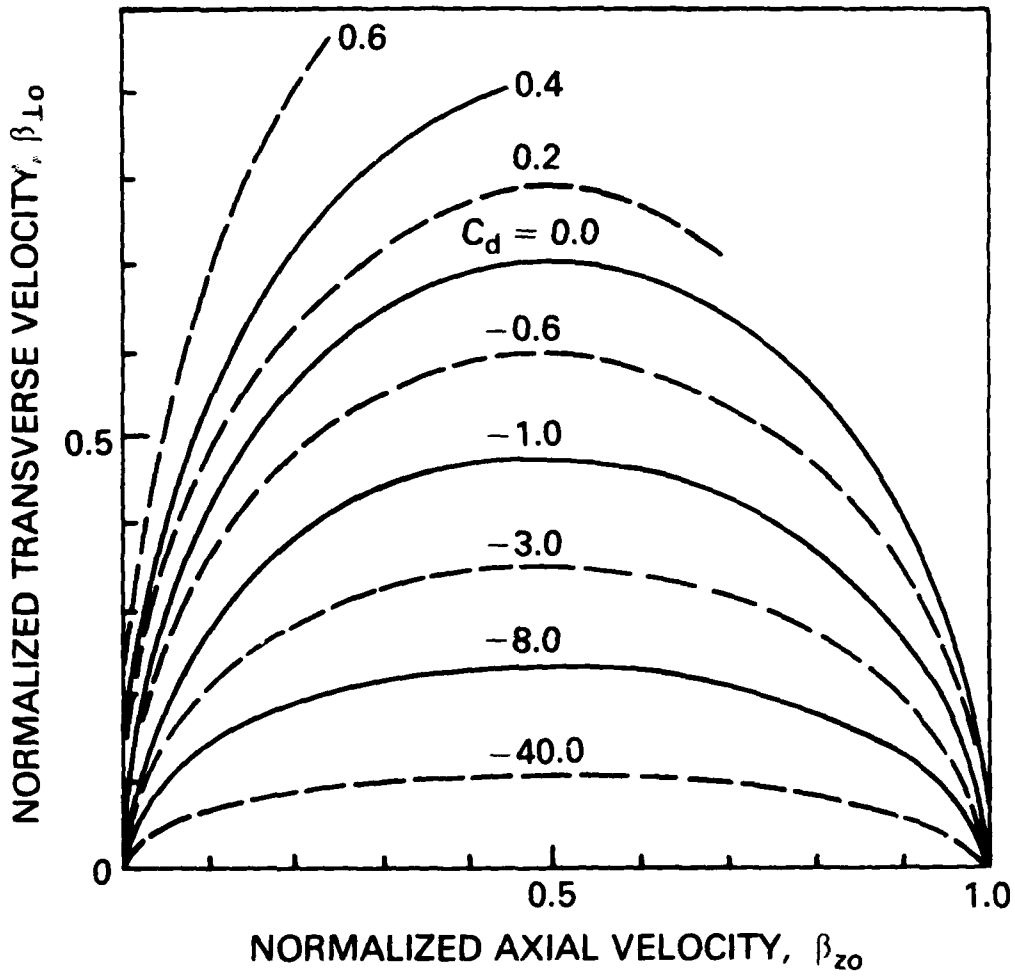

Fig. 6 — Contour plots for the anisotropy constant C_d vs. β_{zo} and $\beta_{\perp o}$.

Let us proceed now to solve for the nonlinear efficiency. Two numerical approaches are available, the first approach based on a numerical integration of the complete set of Eq. (30) to obtain the Lagrangian particle trajectories. The second approach requires the integration of Eq. (43) only. Both approaches have been used. In all cases, the agreement has been excellent. Equally excellent has been the agreement of the results with linear theory, when a sufficiently small amplitude or short interaction length has been employed in the simulations.

The dependence of the normalized efficiency $\eta/C_\eta = 1-\langle q\rangle$ on the reduced distance μ_o is given by the solid curve in Fig. (7) for a distribution characterized by $C_d = -2.5$ and a wave characterized by $C_w = 1.4$. Comparing this curve with linear theory has shown that initially, up to $\mu_o \simeq 1.6$, the evolution is essentially linear. Beyond that point, the efficiency undergoes oscillations in μ_o, reminiscent of the corresponding linear behavior, except that these nonlinear oscillations do not diverge, while the linear result of Eq. (48) predicted divergent oscillations. The location of the relative maxima of the efficiency vs. μ_o is however, in strikingly good agreement with linear theory. The first maximum is at $\mu_o = 3.7$, and the corresponding optimized nonlinear efficiency is $\eta/C_\eta = 0.164$, approximately one half of the linear value $\eta_\ell/C_\eta = 0.300$. For these parameters, subsequent maxima correspond to negative values for the efficiency. The dashed curve corresponds to the values $C_d = -2.5$ and $C_w = 2.7$. This case will be discussed later.

The contour plots of Fig. (8) show the normalized nonlinear efficiency, $1 - \langle q\rangle$, at the first maximum (the one near $\mu_o \simeq 3.7$), for various values of the parameters C_d and C_w. As can be seen from the Figure, large normalized efficiencies, e.g., $1 - \langle q\rangle \cdot 0.15$, are possible

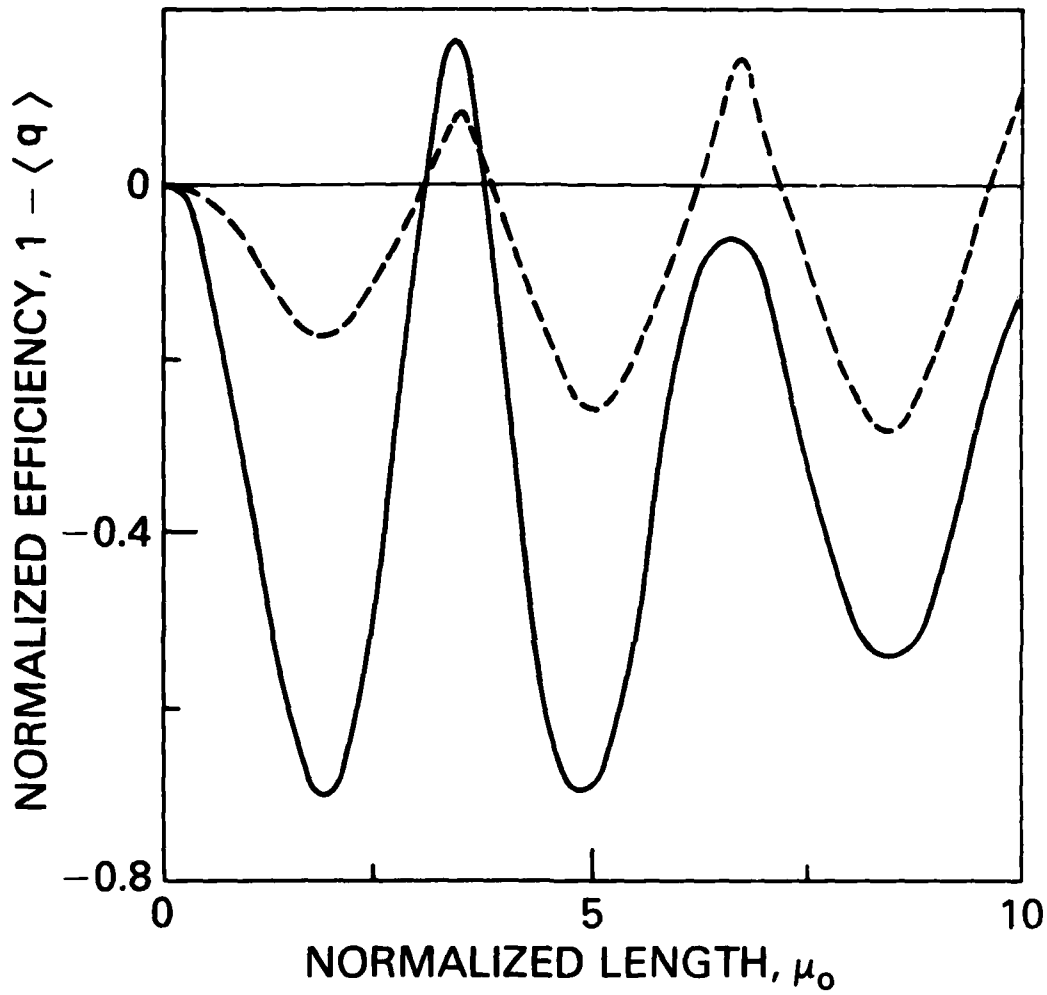

Fig. 7 — Spatial evolution of the normalized efficiency $1-\langle q\rangle = \eta/C_\eta$ for C_d = -2.5 and C_w = 1.4 (solid curve), as well as for C_d = -2.5 and C_w = 2.7 (dashed curve).

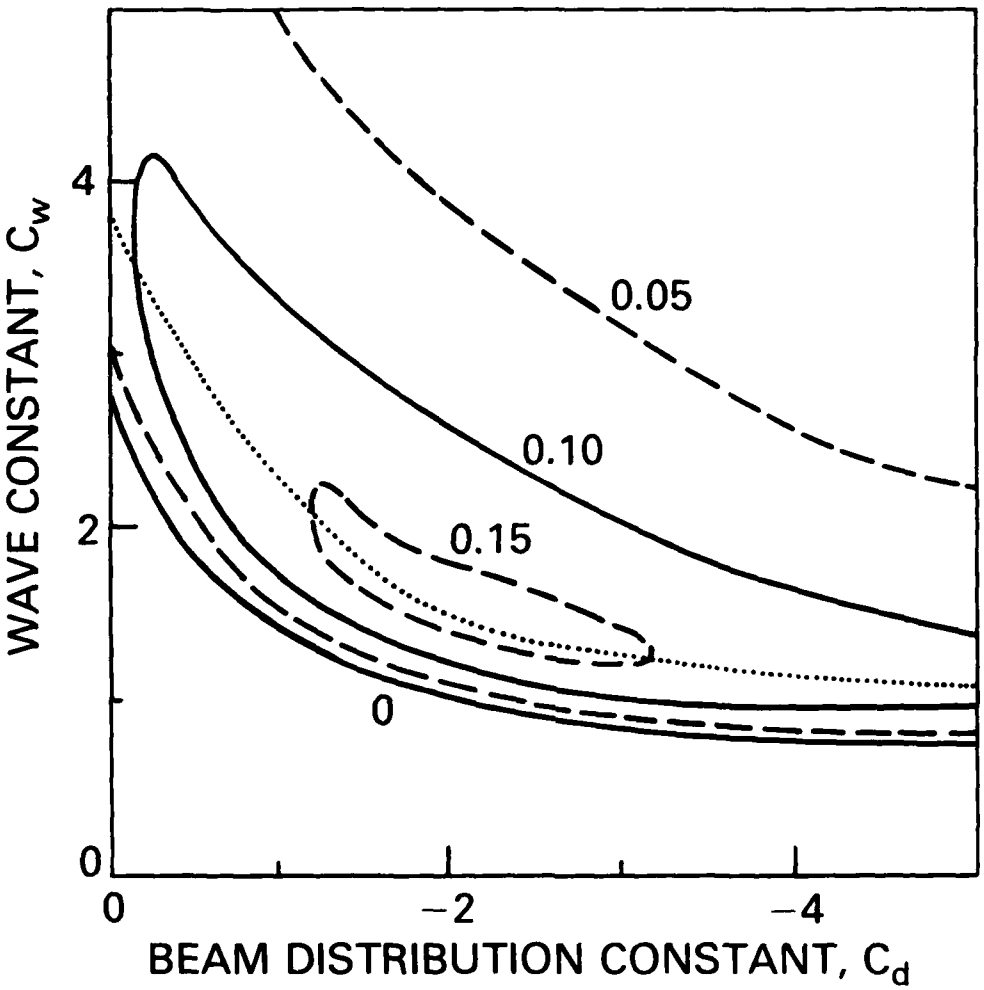

Fig. 8 — Contour plots of the normalized efficiency 1-<q> vs. the parameters C_d and C_w for an interaction length corresponding to the first efficiency maximum ($\mu_o \approx 3.7$). The dotted curve gives the value of C_w for maximum efficiency at any value of C_d.

over a wide range of beam distributions and ratios of frequency mismatch to radiation field amplitude. In addition, the dotted line in Fig. (8) gives the value of C_w required for optimal operation at a given value of C_d. For such values of C_w, the normalized efficiency as a function of C_d is given in Fig. (9). The overall maximum, $1 - \langle q \rangle = 0.165$, is obtained for $C_d = -2.2$, $C_w = 1.5$.

The results presented so far apply to the first maximum of the non-linear efficiency, at a point near $\mu_o = 3.7$. This is not meant to imply that the first efficiency maximum is always dominant. For example, referring again to Fig. (7), it can be seen that increasing the value of C_w, causes the amplitude of the first efficiency maximum to decrease, and that of subsequent maxima to increase. When the point $C_w = 2.7$ is reached (dashed curve), for which $1 - \langle q \rangle$ maximizes near $\mu_o = 6.8$, the normalized nonlinear efficiency is equal to $1 - \langle q \rangle = 0.143$. For even higher values of C_w, it is the third, fourth, etc. efficiency maximum that dominates. The same behavior is observed if $-C_d$ is increased, keeping C_w constant. Contour plots for the efficiency at the second and subsequent maxima are very similar to those of Fig. (8), except that the curves are shifted to slightly higher values of C_w and $-C_d$.

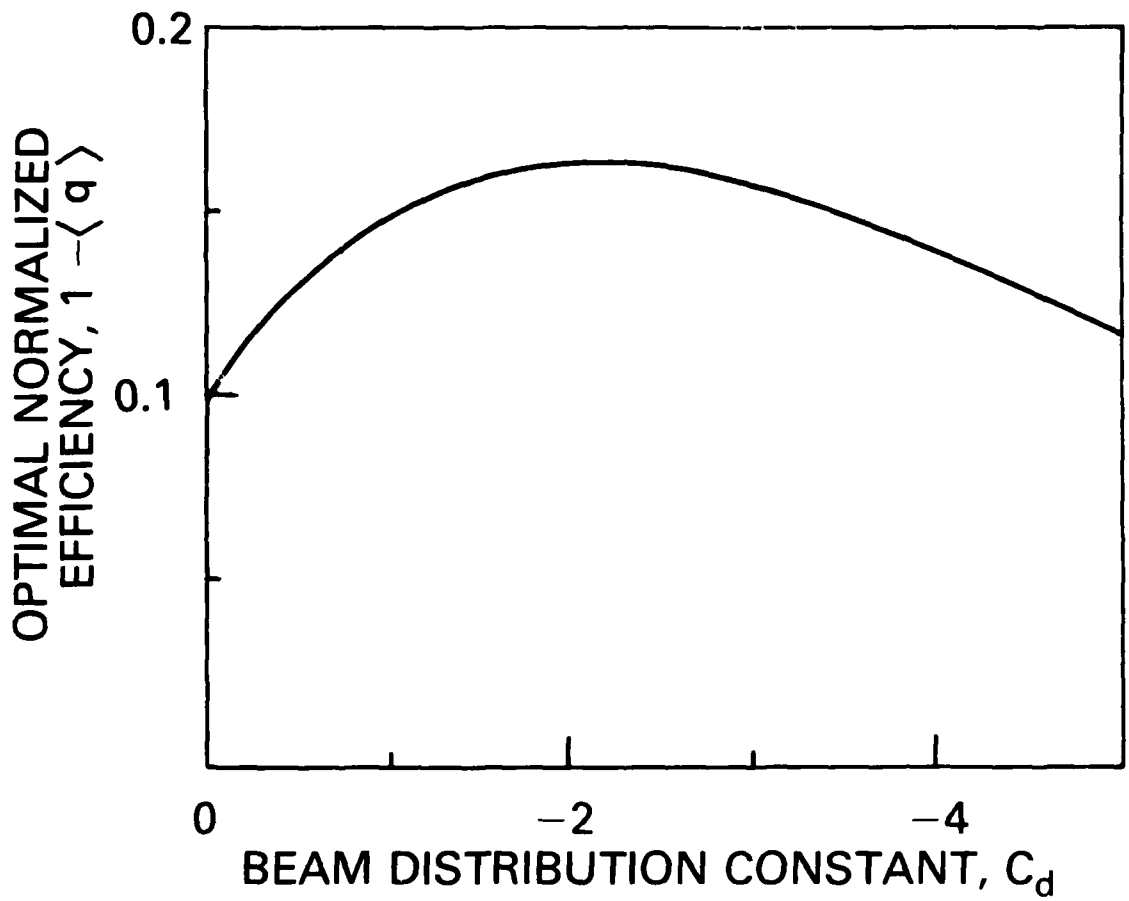

Fig. 9 — Optimal normalized efficiency (i.e., along the dotted curve of Fig. (8)), vs. C_d.

IV. DISCUSSION

In the previous two Sections, we have considered the linear and nonlinear electron cyclotron interaction with (primarily) luminous waves. From that analysis, results have been obtained regarding the stability of these waves and the nonlinear steady-state performance. In this Section, we conclude with various aspects concerning the practical feasibility of a device based on this analysis. We show that this interaction has weak temperature requirements ($\delta\beta_{zo}/\beta_{zo} << 1$) and that excellent mode selection can be achieved. One example of a cyclotron maser is given and the use of this interaction as a free-electron laser is discussed. Finally, the possibility of improving the nonlinear efficiency (up to $\eta \simeq 0.60$) is discussed.

(a) *Temperature requirements*.

Let us consider first the effects associated with a thermal spread, $\delta\beta_{zo}$ and $\delta\gamma_o$, of the beam electrons. The sharpness of the resonance in both linear and nonlinear theory is characterized by the parameter μ_o, which can be written as

$$\mu_o = \pi \frac{L}{\lambda}\left[1 + \frac{\Omega/\gamma_o - \omega}{kc\beta_{zo}}\right] , \tag{49}$$

where $\lambda = 2\pi/k$ is the radiation wavelength. From the dependence of the efficiency on μ_o, it is seen that $|\delta\mu_o| << \pi/4$ is required. With regard to the parallel velocity, this translates to the requirement

$$\frac{\delta\beta_{zo}}{\beta_{zo}} << \frac{1}{4}\,\frac{\lambda}{L}\,\frac{kc\beta_{zo}}{|\Omega/\gamma_o-\omega|} . \tag{50}$$

For conventional cyclotron maser operation, $\omega \gtrsim \Omega/\gamma_0 + kc\beta_{zo}$ and this requirement gives $\delta\beta_{zo}/\beta_{zo} << \lambda/4L$, prohibiting[15] operation in a system longer than a few wavelengths. However, when $\omega = kc$, the symmetry about $\mu_0 = 0$ allows a choice of operating point with $\omega < \Omega/\gamma_0 + kc\beta_{zo}$. In particular, if the wave is suppressed (e.g., by a polygonal ray-path in a multi-mirror resonator) and the choice is made that

$$\mu_0 = \pi \left(\frac{L}{\lambda} + \frac{1}{4}\right) \quad , \tag{51}$$

where a local maximum of the efficiency is located, the requirement is simply

$$\frac{\delta\beta_{zo}}{\beta_{zo}} << 1. \tag{52}$$

For the same operation, the requirement for $\delta\gamma_0$ is

$$\frac{\delta\gamma_0}{\gamma_0} << \frac{1}{4} \; \beta_{zo} \; \frac{\lambda}{L} \quad , \tag{53}$$

which may be more restrictive.

As regards the other significant parameters of the interaction, the requirement $|\delta C_d| << 1 - C_d$ gives a condition supplementary to Eq. (53),

$$\frac{\delta\gamma_0}{\gamma_0} << (\gamma_0\beta_{\perp 0})^2 \quad , \tag{54}$$

while the condition on the parallel velocity is less restrictive than (52). Similarly, the condition $|\delta C_w| << C_w$ is satisfied if the above conditions are satisfied, except that in the highly relativistic limit, $\beta_{zo} \to 1$, an additional condition is imposed, viz.

$$\frac{\delta\beta_{zo}}{\beta_{zo}} << \frac{1-\beta_{zo}}{1-C_d} \quad . \tag{55}$$

(b) Mode Selectivity.

Transverse and longitudinal mode selectivity can be dealt separately. We will not deal in any detail with the former. It is expected that by an appropriate design of the mirrors, only the lowest order transverse mode will be intercepted, while the higher order modes will suffer from diffraction losses.

As far as the longitudinal modes are concerned, we first seek to determine the number of modes that fill the positive gain curve segment, at whose peak the desired longitudinal mode is located. Since the half-width of the gain curve is $|\delta\mu| \lesssim \pi/4$, it can be seen from Eq. (49) that the number $\delta\ell$ of longitudinal mode pairs (in addition to the mode at which operation is desired) within the positive gain segment is

$$\delta\ell \lesssim \frac{\beta_{zo}}{2(1-\beta_{zo})} \quad . \tag{56}$$

Thus, no competing axial modes are present if $\beta_{zo} < 2/3$. On the other hand, many modes will be excited in the case of a highly relativistic electron beam with $\beta_{zo} \to 1$.

An additional point to be considered is whether the operation of the device at a certain efficiency maximum is accompanied by the presence of a different longitudinal mode which might correspond to a value of μ_0 lying within a different positive segment of the gain curve. This question is particularly important when there are many wavelengths within the resonator. In that case, the operation is seen from Eq. (51) to

require a large value of μ_o and the broken line in Fig. (7) indicates that more than one gain segment corresponds to positive gain. Such undesired modes can be suppressed by the introduction of distributed feedback. Inherent means for mode selection are also available. Thus, it can be seen from Eq. (49) that if the choice

$$\beta_{zo} = \frac{1}{2j + 1} \tag{57}$$

is made, where j is an integer, then the closest potentially unstable mode falls at the next (2j-1)-th maximum of the gain curve. If j is not too small, then it is expected that this maximum may correspond to negative gain, thus guaranteeing the absence of any competing modes.

(c) Example of cyclotron maser operation.

Before proceeding, it is necessary to present a numerical example, in order to demonstrate how our results can be applied to a particular design. We consider an interaction at the third maximum of the gain curve. As can be seen from Eq. (51), temperature effects are reduced by choosing a system length equal to 3λ. The normalized efficiency at the third maximum is $\eta/C_\eta = -.156$, for $C_d = -2.9$, $C_w = \pm 3.0$ and $\mu_o = \pm 10.1$. A value $\beta_{zo} = 0.143$ (=1/7) guarantees the absence of any competing modes (see Eq. (57)) and Eq. (53) gives the condition $\delta\gamma_o/\gamma_o << 1.2\%$. From the definition of C_d, Eq. (42) (or, from Fig. (6)), it can be found that $\beta_{\perp o} = 0.25$, hence $\gamma_o = 1.0433$ corresponding to a beam energy of 22.2 keV. Then from the definition of C_η, Eq. (47), or, from Fig. (5), it is found that $C_\eta = 0.88$. Therefore, the nonlinear efficiency is $\eta = 0.137$. For the above values and the definition of C_w (Eq. (40)), the normalized vector potential of the

radiation field, assuming linear polarization, has the value $A_0 = 1.55 \times 10^{-2}$. The external magnetic field gives a gyrofrequency satisfying $\Omega_0/\omega = 1.055$ and the frequency mismatch is $\Delta\omega_0/\omega = (\omega - \Omega_0/\gamma_0 - kv_{z0})/\omega = -0.154$. Finally, by choosing a wavelength $\lambda = 2$ mm, this example requires an external magnetic field of $B_0 = 56.5$ kG for a radiation field amplitude of $E_0 = 833$ sV/cm (= 250 kV/cm) and frequency $\omega = 0.942 \times 10^{12}$ sec^{-1} (= 150 GHz). For an incident beam current of 20 A, the radiated power is 61 kW.

(d) Free-electron-laser type operation.

An interesting variant to the study presented here is the possibility of using the interaction for the excitation of waves with a frequency shifted significantly above the gyrofrequency.[35] It can be seen from the definition of C_W that the frequency is given by

$$\omega = \frac{\Omega_{z0}}{\gamma_0(1-\beta_{z0})} + C_W \frac{1+\varepsilon}{\gamma_0\beta_{\perp 0}} \frac{eE_0}{mc} , \tag{58}$$

where $E_0 = \omega A_0/c$ is the amplitude of the electric component of the radiation field. The operating frequency is essentially given by the first term in Eq. (58). Defining the axial relativistic factor, $\gamma_{z0}=(1-\beta_{z0}^2)^{-1/2}$, the operating frequency is accurately given by

$$\omega = (1 + \beta_{z0})\gamma_{z0}^2 \frac{\Omega_0}{\gamma_0} \tag{59}$$

and bears the same form as the free-electron laser frequency,[36,37] employing a magnetic wiggler.

Since the relativistic gyrofrequency depends on the mass factor γ_0, the actual quantity that multiplies the nonrelativistic gyrofrequency to give the operating frequency is I_1^{-1}, where $I_1 = \gamma_0(1-\beta_{z0})$ is the first invariant. For high operating frequencies, it is required that $I_1^{-1} >> 1$. This requirement, together with the desire that C_η be not too much less than unity (in order to achieve adequate efficiencies) requires that $-C_d << 1$. Thus, as can be seen from Fig. (9), efficiencies of the order of 10% are to be expected. For example, $\omega/\Omega_0 = 10$ requires $I_1 = 0.1$. Taking $\gamma_0 = 50$, gives $\beta_{z0} = 0.998$ and $\beta_{\perp 0} = 0.06$. Then $C_d = -0.11$, giving $\eta/C_\eta = 0.102$, and $C_\eta = 0.917$, and the result is an efficiency $\eta = 9.36\%$. (Of course, higher efficiencies can be obtained by adopting efficiency enhancement schemes, as discussed in IV(e) below.) In this example, it is required that $C_w = 3.6$ and $\mu_0 = 3.6$. Choosing a wavelength of λ=0.2 mm (f = 1.5 THz) and a system length L = 1m = 5000 λ, it is found that an external magnetic field of strength B_0 = 47.5 kGs is needed. Furthermore, assuming a beam current of 10 A, the radiated power is equal to P_{rad} = 23.4 MW.

(e) Efficiency enhancement.

The nonlinear analysis of Sec. III shows that the performance of an oscillator operating with luminous waves is limited to efficiencies $\eta \lesssim 16\%$. Here we will outline briefly a scheme which can improve the performance of the interaction dramatically. We introduce a two-stage oscillator configuration, in which the first stage (the prebuncher) acts to pre-bunch the particles in their relative angle χ, without significantly changing particle momentum. The second stage (the converter) converts the kinetic energy of the bunch to radiation energy. A 100% conversion

is possible, if the bunch is perfect and $C_d = 0$.

In the prebuncher we require a combination of a "large" frequency mismatch and "small" radiation field amplitude, such that $|C_{w1}| >> 1$. In this stage the electrons are highly untrapped and only negligible energy exchange occurs. To first order χ is

$$\chi^{(1)} = \chi_o + \left(C_{w1} - \frac{\cos\chi_o}{2}\right)\zeta \tag{60}$$

where $C_d = 0$ has been assumed. For χ_o uniformly distributed in the interval $(0, 2\pi)$, Eq. (60) describes the formation of a bunch.

The extraction of particle energy occurs in the converter. From the discussion of Sec. III (see also Fig. (3)), it is recalled that a particle on the separatrix eventually loses all its kinetic energy, if $C_d = 0$, as is assumed here. Since the bunch has a spread in χ rather than in q, it is necessary to arrange the converter parameters so that $C_{w2} = 1$. With an appropriate choice of C_{w1}, the bunch will be centered at the peak of the separatrix. The center of the bunch will thus be able to convert all its energy to radiation energy, by choosing the appropriate length for the converter section. Examining the bunch coherence from Eq. (60) it can be estimated that efficiencies of the order of 60% are attainable.

As an example of a two-stage oscillator we consider the case $C_{w1} = 7.5$, $C_d = 0$, with a discontinuity in the radiation field amplitude, $C_{w2} = 1.0$, for $\zeta > \zeta_1$. The evolution of the efficiency for this case is shown in Fig. (10). The oscillatory curve gives the evolution when the first oscillator is sufficiently long, $\zeta_1 \to \infty$. However, if the location of the discontinuity is appropriately chosen, the ensuing evolution is

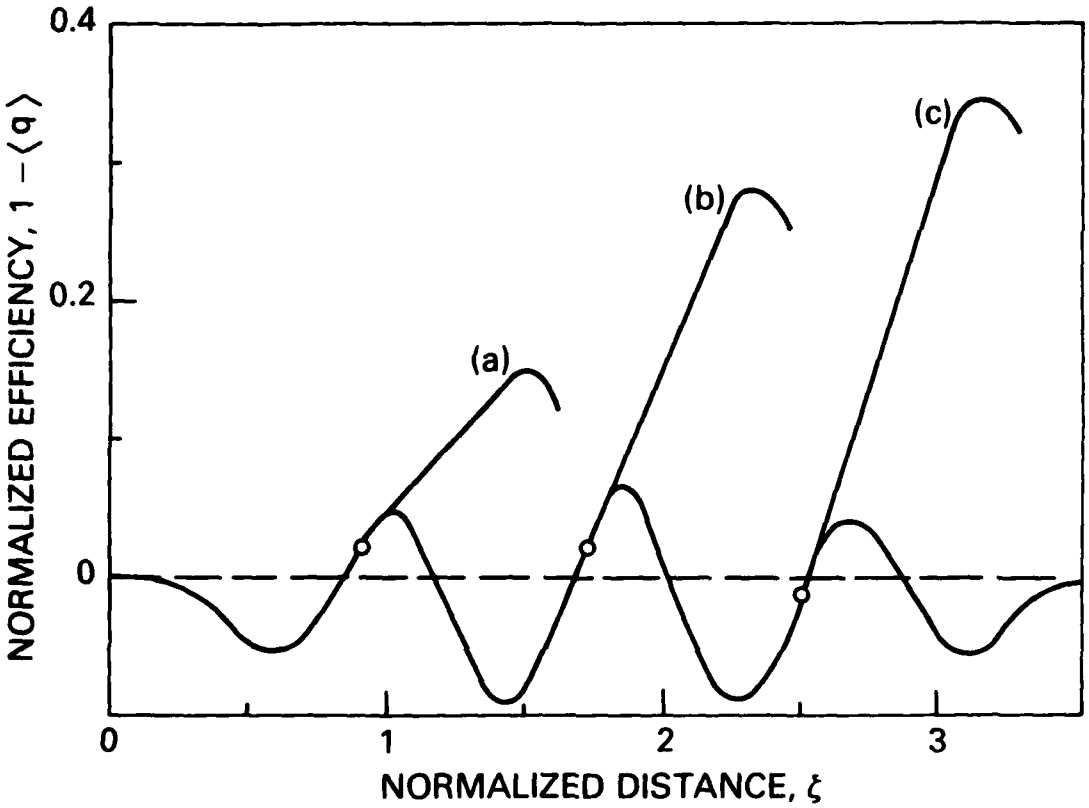

Fig. 10 — Efficiency enhancement in a two-stage oscillator configuration. The oscillatory curve gives the nonlinear normalized efficiency vs. normalized distance for $C_{w1} = 7.5$ and $C_d = 0$ in a single resonator. The introduction of a second resonator with $C_{w2} = 1.0$ at $\zeta = \zeta_1$, shown by the small circles, improves the overall efficiency. The cases shown correspond to (a) $\zeta_1 = 0.90$, (b) $\zeta_1 = 1.72$, and (c) $\zeta_1 = 2.50$.

characterized by substantially increased efficiency. Thus, for the choices ζ_1 = 0.90, 1.72, and 2.50, shown in the figure by the small circles, the evolution of the efficiency in the second oscillator, where C_{w2} = 1.0, is shown by the curves (a), (b), and (c). This procedure yields the optimal values of the efficiency η = 0.15, 0.28, and 0.35 at the positions ζ_2 = 1.5, 2.3, and 3.1, respectively. This clearly demonstrates the principle of efficiency enhancement in a two-stage oscillator.

ACKNOWLEDGMENTS

This work has been supported by the Office of Naval Research and the U. S. Department of Energy. Discussions with W. M. Manheimer have been very useful.

REFERENCES

1. R. Q. Twiss, Australian J. Phys. 11, 564 (1958).

2. A. V. Gaponov, Izv. VUZ. Radiofizika, 2, 450 (1959).

3. R. H. Pantell, Proc. IRE, 47, 1146(1959).

4. J. L. Hirschfield, I. B. Bernstein, and J. M. Wachtel, IEEE J. Quantum Electron., QE-1, 237(1965).

5. A. V. Gaponov, M. I. Petelin, and V. K. Yulpatov, Radiophys. Quantum Electron, 10, 794 (1967).

6. M. Borenstein and W. E. Lamb, Jr., Phys. Rev., A5, 1298 (1972).

7. Edward Ott and Wallace M. Manheimer, IEEE Trans. PS-3, 1 (1975).

8. P. Sprangle and Wallace M. Manheimer, Phys. Fluids 18, 224 (1975).

9. V. L. Granatstein, P. Sprangle, M. Herndon and R. K. Parker, J. Applied Phys. 46, 2021 (1975).

10. V. A. Flyagin, A. V. Gaponov, M. I. Petelin, and V. K. Yulpatov, IEEE Trans. MTT-25, 514 (1977).

11. J. L. Hirshfield and V. L. Granatstein, IEEE Trans. MTT-25, 522 (1977).

12. P. Sprangle and A. T. Drobot, IEEE Trans. MTT-25, 528 (1977).

13. W. M. Manheimer and V. L. Granatstein, NRL Memorandum Report 3493 (1977).

14. A. A. Andronov, V. A. Flyagin, A. V. Gaponov, A. L. Gol'denberg, M. I. Petelin, V. G. Usov, and V. K. Yulpatov, Infrared Physics 18, 385 (1978).

15. H. Jory, S. Hegji, J. Shiverly and R. Symons, Microwave J. 21, 30 (1978).

16. K. R. Chu, Phys. Fluids 21, 2354 (1978).

17. J. L. Seftor, V. L. Granatstein, K. R. Chu, P. Sprangle and M. E. Read, IEEE J. Quantum Electron., QE-15, 849 (1979).

18. M. E. Read, R. M. Gilgenbach, R. Lucey, Jr., K. R. Chu, A. T. Drobot and V. L. Granatstein, IEEE Trans. MTT (in press).

19. D. V. Kisel', G. S. Korablev, V. G. Navel'yev, M. I. Petelin, and Sh. Ye. Tsimring, Radio Engineering and Electronics Physics 19, 95 (1974).

20. Yu. V. Bykov and A. L. Gol'denberg, Radiophys. Quantum Electron. 18, 791 (1975).

21. P. Sprangle and Robert A. Smith, NRL Memorandum Report 3983 (1979).

22. K. R. Chu, M. E. Read, and A. K. Ganguly, NRL Memorandum Report 4051 (1979).

23. M. E. Read, K. R. Chu, and A. J. Dudas, NRL Memo Rpt. 4169 (1980).

24. M. A. Moiseev, G. S. Nusinovich, Radiophys. Quantum Electron. 17, 1305 (1974).

25. G. S. Nusinovich, Radiophys. Quantum Electron. 19, 1301 (1976).

26. I. G. Zarnitsyna and G. S. Nusinovich, Radiophys. Quantum Electron. 20, 313 (1977).

27. J. L. Vomvoridis and P. Sprangle, NRL Memorandum Report 4426 (1980).

28. D. J. Dialetis and K. R. Chu, NRL Memorandum Report

29. The case of the electron beam propagating across the resonator axis is considered in P. Sprangle, W. M. Manheimer and J. L. Vomvoridis, NRL Memorandum Report 4366(1980); also submitted to Phys. Rev. A.

30. The backward wave can be suppressed by a multi-mirror resonator arrangement, in which the radiation follows a polygonal path. Also, the effects of the backward wave are negligible when $\Delta\omega << kv_{\parallel}$.

31. K. R. Chu and J. L. Hirshfield, Phys. Fluids 21, 461 (1978).

32. S. K. Ride and W. B. Colson, Appl. Phys. 20, 41 (1979).

33. C. S. Roberts and S. J. Buchsbaum, Phys. Rev. 135, A381 (1964).

34. R. F. Lutomirski and R. N. Sudan, Phys. Rev. 147, 156 (1966).

35. J. L. Hirshfield, K. R. Chu and S. Kainer, Appl. Phys. Lett. 33, 847 (1978).

36. P. Sprangle and R. A. Smith, Phys. Rev. A21, 293 (1980).

37. P. Sprangle, Cha-Mei Tang and W. M. Manheimer, Phys. Rev. A21, 302 (1980).

DISTRIBUTION LIST*

Naval Research Laboratory
4555 Overlook Avenue, S.W.
Washington, D.C. 20375

Attn: Code 1000 - CAPT E. E. Henifin
1001 - Dr. A. Berman
4700 - Dr. T. Coffey (25 copies)
4701 - Mr. J. Brown
4740 - Dr. V. L. Granatstein (20 copies)
4740 - Dr. K. R. Chu
4740 - Dr. C. W. Roberson
4740 - Dr. M. E. Read
4790 - Dr. P. Sprangle (100 copies)
4790 - Dr. M. Lampe
4790 - Dr. W. M. Manheimer
6603S- Dr. W. W. Zachary
6650 - Dr. L. Cohen
6656 - Dr. N. Seeman
6805 - Dr. S. Y. Ahn
6805 - Dr. A. Ganguly
6805 - Dr. N. R. Vanderplaats
6850 - Dr. L. R. Whicker
6875 - Dr. R. Wagner

On Site Contractors:

Code 4740 - Dr. J. M. Baird (B-K Dynamics)
4740 - Dr. L. Barnett (B-K Dynamics)
4740 - Dr. D. Dialetis (SAI)
4740 - Dr. Y. Y. Lau (SAI)
4740 - Dr. J. S. Silverstein (HDL)
4790 - Dr. A. T. Drobot (SAI)
4790 - Dr. C. M. Tang (JAYCOR)
4790 - Dr. J. Vomvoridis (JAYCOR)(50 copies)
4790 - Dr. H. Freund (SAI)

* Every name listed on distribution gets one copy except for those where extra copies are noted.

Dr. Tony Armstrong
SAI, Inc.
P. O. Box 2351
La Jolla, CA 92038

Dr. Robert Behringer
ONR
1030 E. Green
Pasadena, CA 91106

Dr. G. Bekefi (5 copies)
Massachusetts Institute of Technology
Bldg. 26
Cambridge, MA 02139

Dr. Arden Bement (2 copies)
Deputy Under Secretary of
Defense for R&AT
Room 3E114, The Pentagon
Washington, D.C. 20301

Dr. T. Berlincourt
Code 420
Office of Naval Research
Arlington, VA 22217

Dr. I. B. Bernstein (2 copies)
Yale University
Mason Laboratory
400 Temple Street
New Haven, CT 06520

Dr. Fred Burskirk
Physics Department
Naval Postgraduate School
Monterey, CA 93940

Dr. K. J. Button
Massachusetts Institute of Technology
Francis Bitter National Magnet
Laboratory
Cambridge, MA 02139

Dr. Gregory Canavan
Director, Office of Inertial Fusion
U. S. Department of Energy
M.S. C404
Washington, D.C. 20545

Dr. C. D. Cantrell
T-DOT, MS210
Los Alamos Scientific Laboratory
Los Alamos, NM 87545

Dr. Weng Chow
Optical Sciences Center
University of Arizona
Tucson, AZ 85721

Dr. Peter Clark
TRW, Building R-1, Room 1096
One Space Park
Redondo Beach, CA 90278

Dr. Robert Clark
P. O. Box 1929
Washington, D.C. 20013

Dr. William Colson
Quantum Institute
Univ. of California at Santa Barbara
Santa Barbara, CA 93106

Dr. William Condell
Code 421
Office of Naval Research
Arlington, VA 22217

Dr. Richard Cooper
Los Alamos Scientific Laboratory
P. O. Box 1663
Los Alamos, NM 87545

Cmdr. Robert Cronin
NFOIO Detachment, Suitland
4301 Suitland Road
Washington, D.C. 20390

Dr. R. Davidson (5 copies)
Plasma Fusion Center
Massachusetts Institute of Technology
Cambridge, MA 02139

Dr. John Dawson (2 copies)
Physics Department
University of California
Los Angeles, CA 90024

Defense Technical Information Center
(12 copies)
Cameron Station
5010 Duke Street
Alexandria, VA 22313

Dr. Francesco De Martini
Instituto de Fiscia
"G. Marconi" Univ.
Piazzo delle Science, 5
ROMA00185 ITALY

Prof. P. Diament
Columbia University
Dept. of Electrical Engineering
New York, NY 10027

Prof. H. J. Doucet (5 copies)
Ecole Polytechnique
91128 Palaiseau
Paris, France

Dr. John Elgin (2 copies)
Imperial College
Dept. of Physics (Optics)
London SWF, England

Dr. David D. Elliott
SRI International
333 Ravenswood Avenue
Menlo Park, CA 94025

Dr. Norval Fortson
Department of Physics
University of Washington
Seattle, WA 98195

Director (2 copies)
National Security Agency
Fort Meade, MD 20755
ATTN: Mr. Richard Foss, A42

Dr. Robert Fossum, Director
(2 copies)
DARPA
1400 Wilson Boulevard
Arlington, VA 22209

Dr. Edward A. Frieman
Director, Office of Energy Research
U. S. Department of Energy
M.S. 6E084
Washington, D.C. 20585

Dr. George Gamota (3 copies)
OUSDRE (R&AT)
Room 3D1067, The Pentagon
Washington, D.C. 20301

Dr. Richard L. Garwin
IBM, T. J. Watson Research Center
P. O. Box 218
Yorktown Heights, NY 10598

Dr. Edward T. Gerry, President
W. J. Schafer Associates, Inc.
1901 N. Fort Myer Drive
Arlington, VA 22209

Dr. Avraham Gover
Tel Aviv University
Fac. of Engineering
Tel Aviv, ISRAEL

Dr. A. H. Guenter
Chief Scientist
Air Force Weapons Laboratory
Kirtland AFB, NM 87117

Mr. Donald L. Haas, Director
DARPA/STO
1400 Wilson Boulevard
Arlington, VA 22209

Dr. P. Hammerling
La Jolla Institute
P. O. Box 1434
La Jolla, CA 92038

Director
National Security Agency
Fort Meade, MD 20755
ATTN: Mr. Thomas Handel, A243

Dr. William Happer
560 Riverside Drive
New York City, NY 10027

Dr. Robert J. Hermann
Assistant Secretary of the
Air Force (RD&L)
Room 4E856, The Pentagon
Washington, D.C. 20330

Dr. Rod Hiddleston
KMS Fusion
Ann Arbor, MI 48106

Dr. J. L. Hirshfield (2 copies)
Yale University
Mason Laboratory
400 Temple Street
New Haven, CT 06520

Dr. R. Hofland
Aerospace Corp.
P. O. Box 92957
Los Angeles, CA 90009

Dr. Benjamin Huberman
Associate Director, OSTP
Room 476, Old Executive Office Bldg.
Washington, D.C. 20506

Dr. S. F. Jacobs
Optical Sciences Center
University of Arizona
Tucson, AZ 85721

Dr. Howard Jory (3 copies)
Varian Associates, Bldg. 1
611 Hansen Way
Palo Alto, CA 94303

Mr. Eugene Kopf
Principal Deputy Assistant
Secretary of the Air Force (RD&L)
Room 4E964, The Pentagon
Washington, D.C. 20330

Prof. N. M. Kroll
La Jolla Institutes
P. O. Box 1434
La Jolla, CA 92038

Dr. Tom Kuper
Optical Sciences Center
University of Arizona
Tucson, AZ 85721

Dr. Willis Lamb
Optical Sciences Center
University of Arizona
Tucson, AZ 85721

Mr. Mike Lavan
BMDATC-O
ATTN: ATC-O
P. O. Box 1500
Huntsville, AL 35807

Dr. John D. Lawson (2 copies)
Rutherford High Energy Lab
Chilton
Didcot, Oxon OX11 00X
ENGLAND

Mr. Ray Leadabrand
SRI International
333 Ravenswood Avenue
Menlo Park, CA 94025

Mr. Barry Leven
NISC/Code 20
4301 Suitland Road
Washington, D.C. 20390

Dr. Donald M. LeVine (3 copies)
SRI International
1611 N. Kent Street
Arlington, VA 22209

Dr. Anthony T. Lin
University of California
Los Angeles, CA 90024

Director (2 copies)
National Security Agency
Fort Meade, MD 20755
ATTN: Mr. Robert Madden, R/SA

Dr. Joseph Mangano
DARPA
1400 Wilson Boulevard
Arlington, VA 22209

Dr. S. A. Mani
W. J. Schafer Associates, Inc.
10 Lakeside Office Park
Wakefield, MA 01880

Dr. Mike Mann
Hughes Aircraft Co.
Laser Systems Div.
Culver City, CA 90230

Dr. T. C. Marshall
Applied Physics Department
Columbia University
New York, NY 10027

Mr. John Meson
DARPA
1400 Wilson Boulevard
Arlington, VA 22209

Dr. Pierre Meystre
Projektgruppe fur Laserforschung
Max Planck Gesellschaft
Garching, Munich GERMANY

Dr. Gerald T. Moore
Optical Sciences Center
University of Arizona
Tucson, AZ 85721

Dr. Philip Morton
Stanford Linear Accelerator Center
P. O. Box 4349
Stanford, CA 94305

Dr. Jesper Munch
TRW
One Space Park
Redondo Beach, CA 90278

Dr. George Neil
TRW
One Space Park
Redondo Beach, CA 90278

Dr. Kelvin Neil
Lawrence Livermore Laboratory
Code L-321, P. O. Box 808
Livermore, CA 94550

Dr. Milton L. Noble (2 copies)
General Electric Company
G. E. Electronic Park
Syracuse, NY 13201

Prof. E. Ott (2 copies)
University of Maryland
Dept. of Physics
College Park, Md. 20742

Dr. Richard H. Pantell
Stanford University
Stanford, CA 94305

Dr. Richard M. Patrick
AVCO Everett Research Lab., Inc.
2385 Revere Beach Parkway
Everett, MA 02149

The Honorable William Perry
Under Secretary of Defense (R&E)
Office of the Secretary of Defense
Room 3E1006, The Pentagon
Washington, D.C. 20301

Dr. Alan Pike
DARPA/STO
1400 Wilson Boulevard
Arlington, VA 22209

Dr. Hersch Pilloff
Code 421
Office of Naval Research
Arlington, VA 22217

Dr. Charles Planner
Rutherford High Energy Lab
Chilton
Didcot, Oxon, OX11 OOX,
ENGLAND

Dr. Michal Poole
Daresbury Nuclear Physics Lab.
Daresbury, Warrington
Cheshire WA4 4AD
ENGLAND

Dr. Don Prosnitz
Lawrence Livermore Laboratory
Livermore, CA. 94550

Dr. D. A. Reilly
AVCO Everett Research Lab.
Everett, MA 02149

Dr. James P. Reilly
W. J. Schafer Associates, Inc.
10 Lakeside Office Park
Wakefield, MA 01880

Dr. A. Renieri
C.N.E.N.
Div. Nuove Attivita
Dentro di Frascatti
Frascatti, Rome
ITALY

Dr. Daniel N. Rogovin
SAI
P. O. Box 2351
La Jolla, CA 92038

Dr. Michael Rosenbluh
MIT - Magnet Lab.
Cambridge, MA 02139

Dr. Marshall N. Rosenbluth
Institute for Advanced Study
Princeton, NJ 08540

Dr. Eugene Ruane (2 copies)
P. O. Box 1925
Washington, D.C. 20013

Dr. Antonio Sanchez
MIT/Lincoln Laboratory
Room B231
P. O. Box 73
Lexington, MA 02173

Prof. S. P. Schlesinger
Columbia University
Dept. of Electrical Engineering
New York, NY 10027

Dr. Howard Schlossberg
AFOSR
Bolling AFB
Washington, D.C. 20332

Dr. Stanley Schneider
Rotodyne Corporation
26628 Pond Du Lac Road
Palos Verdes Peninsula, CA 90274

Dr. Marlan O. Scully
Optical Sciences Center
University of Arizona
Tucson, AZ 85721

Dr. Robert Sepucha
DARPA/STO
1400 Wilson Boulevard
Arlington, VA 22209

Dr. A. M. Sessler
Lawrence Berkeley Laboratory
University of California
1 Cyclotron Road
Berkeley, CA 94720

Dr. Earl D. Shaw
Bell Labs
600 Mountain Avenue
Murray Hill, NJ 07974

Dr. Chan-Ching Shih
R&D Associates
P. O. Box 9695
Marina del Rey, CA 92091

Dr. Kenneth Smith
Physical Dynamics, Inc.
P. O. Box 556
La Jolla, CA 92038

Mr. Todd Smith
Hansen Labs
Stanford University
Stanford, CA 94305

Dr. Joel A. Snow
Senior Technical Advisor
Office of Energy Research
U. S. Department of Energy, M.S. E084
Washington, D.C. 20585

Mrs. Alma Spring
DARPA/Administration
1400 Wilson Boulevard
Arlington, VA 22209

SRI/MP Reports Area G037 (2 copies)
333 Ravenswood Avenue
Menlo Park, CA 94025
ATTN: D. Leitner

Dr. Abraham Szoke
Lawrence Livermore Laboratory
MS L-470, P. O. Box 808
Livermore, CA 94550

Dr. Milan Tekula
AVCO Everett Research Lab.
2385 Revere Beach Parkway
Everett, MA 02149

Dr. R. Temkin (2 copies)
Plasma Fusion Center
Massachusetts Institute of Technology
Cambridge, MA 02139

Dr. John E. Walsh
Department of Physics
Dartmouth College
Hanover, NH 03755

Dr. Wasneski (2 copies)
Naval Air Systems Command
Department of the Navy
Washington, D.C. 20350

Lt. Col. W. Whitaker
Defense Advanced Research Projects
Agency
1400 Wilson Boulevard
Arlington, VA 22209

Ms. Bettie Wilcox
Lawrence Livermore Laboratory
ATTN: Tech. Info. Dept. L-3
P. O. Box 808
Livermore, CA 94550

Dr. A. Yariv
California Institute of Tech.
Pasadena, CA 91125

ATE

LMED

-8